Energy 165 (2018) 483–500

Contents lists available at ScienceDirect

Energy

journal homepage: www.elsevier.com/locate/energy

Two-step optimization procedure for the conceptual design of A-frame systems for solar power plants

José A. Luceño, Mariano Martín*

Departamento de Ingeniería Química y Textil, Universidad de Salamanca, Pza. Caídos 1-5, 37008, Salamanca, Spain

ARTICLE INFO

Article history:
Received 15 June 2017
Received in revised form
27 August 2018
Accepted 27 September 2018
Available online 28 September 2018

Keywords:
Energy
Concentrated solar power
A-frame
Dry cooling
Mathematical optimization
Operation

ABSTRACT

This work presents a two-stage optimization procedure for the conceptual design and operation of A-frame dry cooling systems for concentrated solar power facilities. First, the optimal geometry of the A-frame including sizing, number of fans and blade geometry, and unit parameters such as pipe length, configuration and number is determined. Finally, the operation of the system over a year for minimum energy consumption is computed. The geometry problem is formulated as a mixed-integer non linear programming (MINLP) problem. A tailor-made branch and bound algorithm is used to solve the complex non-linear programming sub-problems. The second problem consists of a multi-period MINLP. A fixed geometry is used to evaluate the usage of fans over time. The solution suggests an apex angle of 63°, one row of 75 pipes of 13.5 *m* long with a diameter of 3.3 mm, and 4 fans are used but they only operate at full capacity during summer. This design allows reducing the energy required by 20% by using the appropriate pipe configuration and number. The unit consumes around 4% of the energy produced by the CSP plant that serves. It is a promising result that can be affected by plant layout and ground availability.

1. Introduction

Solar energy is a plentiful source that can provide several times the mankind needs [1]. However, the use of solar energy to produce power is still not competitive compared to fossil based thermal plants [2]. The disadvantage of concentrated solar power facilities (CSP) is that, unlike fossil based ones, they need to be allocated in specific regions with high solar incidence. This particular feature is a handicap in terms of cooling. There are two main cooling technologies for thermal plants: wet or dry cooling. Wet cooling is the most used technology for power plants, but it requires around 1.8 L of water per kWh produced [2]. On the other hand, dry cooling technologies require the use of a fraction of the power generated to operate the fans that move the air used to condensate the exhaust steam. As a result, the global efficiency of the facility is reduced.

In the literature, a number of studies compare wet and dry cooling systems for solar and fossil based thermal plants. Most of them use a simulation based approach to compare power plants that use both cooling technologies. Kelly and Prince [3] evaluated the performance of air cooled condensers using the Excelergy package and compared the cost of power production using both cooling systems showing that dry is still more expensive. Turchi et al. [4] studied 13 different real cases using SAM software, where the use of dry cooling increased the cost of electricity by 8%, but with reduction of water consumption of 90% in CSP plants. No details on the air cooler geometry are presented. Zhai and Rubin [5] focused on comparing the cost and performance of both cooling technologies on coal based facilities. A-frame coolers are used but no details of the unit are described. Barigozzi et al. [6] optimized wet and dry cooling systems for waste-to-energy plants evaluating the effect of air conditions on the cycle performance using Thermoflex software, but no unit design characteristics are commented. Blanco-Marigorta et al. [7] used exergy as metric to compare both technologies in terms of thermodynamic yield of the process. Habl et al. [8] extended previous work by including cost estimation. Liqreina [9] only focused on dry systems for a CSP plant located in a desert area, Jordan, from the thermodynamic poinf of view. Palenzuela et al. [10] evaluated various cooling technologies in the context of desalination. Lately, a programming optimization approach has been used to evaluate wet, Martín and Martín [2], and dry cooling systems Martín [11] towards the trade-off between water consumption and power generation. A monthly basis analysis is performed. Dry cooling technologies reported higher power production and investment costs. Around 5–10% of the produced

* Corresponding author.
E-mail address: mariano.m3@usal.es (M. Martín).

https://doi.org/10.1016/j.energy.2018.09.177
0360-5442/

energy is consumed to power the fans using dry cooling technologies [11], while the use of wet cooling towers resulted in an average consumption of 2.1 L/kWh of water [2]. Cooling technologies have been developed lately not only for renewable based power plants but also to address residential needs evaluating system [12], comparing previous work with air cooling [13] and finally evaluating various renewable resources [14]. However, these studies used simplified models to represent the cooling technologies in order to be able to address the analysis or the optimization of the entire power facilities. The increase in power demand together with the future water scarcity [15] requires better dry cooling systems [16].

Literature on the design of dry cooling systems focuses on different aspects. Some studies evaluate the layout of the units for their allocation in the facility using Computational Fluid dynamics (CFD), suggesting novel layouts [17] and evaluating the effect of wind speed direction [18]. In terms of the actual unit design, two approaches can be found in the literature, iterative design and mathematical optimization formulations. The most common approach uses guidelines, figures and design equations in an interative procedure. The general rules can be found in technical reports [19], or reference books where the design procedure is described in detail in Ref. [20]. Industry also provides their guidelines based on the experience on the operation of such units [21]. Apart from the basic design, the effect of the wind can also be accounted for in the design [22]. Finally, specific problems such as freezing [23], or the evaluation of the fan performance with no further reference to the entire design and the heat transfer section [24] have also been considered. Alternatively, mathematical optimization approaches have been developed. However, most of these studies have been performed for regular units either evaluating their performance [25] or developing a mathematical model for their optimization [26]. The optimization of the particular geometry of the A-frames has only been addressed in Ref. [27] for a reduced number of variables. Conradie's et al. work [27] used a mathematical optimization approach for the geometric design of A-frame systems. However, it does not evaluate the effect on the flow on the heat transfer coefficients, the effects of the geometry on the pressure drop nor its operation over a year time.

Apart from the geometrical design of the unit, the variability in the solar incidence represents the second challenge in the operation of CSP plants. In particular, cooling units are affected in two ways, the variable heat load to be rejected and the variable conditions of the cooling agent. Typically, the design is based on a certain month of operation [20], but in the case of solar facilities this approach leads to inefficiencies over a year. Even though flexible design of chemical plants has been addressed in the literature using mathematical optimization approaches [28], its application to the detailed design of industrial units considering the monthly variability is challenging due to the mathematical complexity. Reference to multi-period operation can be found in some studies that evaluate the performance for regular air coolers [26] or that focuses on the evolution of fouling and its effect on the energy transfer [29], but work on the detail optimal design of A-frames considering seasonality operation is not available.

In this work a two-stage methodology has been proposed for the conceptual optimal geometric design and monthly operation of A-frames aiming at minimum power consumption to meet the cooling needs of a CSP plant. The methodology is based on the detailed geometric design for a month considering the piping system and its layout, the fan blade geometry, pressure drop across the system and heat transfer resistances. Next, as a recourse, the second step a multiperiod optimization allows considering the operation of such design over time to minimize energy consumption The aim is to improve current designs reducing the energy required to operate such units. For reference, the case study is based on a CSP facility located in Almería (Spain), a region with one of the highest solar radiations in Europe, and uses operating data from previous work [2]. The paper is organized as follows: In Section 2, the design method is depicted. In Section 3, the features of the model are described. In Section 4 the optimization procedure developed to solve the MINLP problem is presented. Next, in Section 5 the case study and the main results are discussed such as the major operating conditions, the power consumed by the cooling system and the units of the A-frame needed followed by an economic evaluation and a comparison between dry and wet cooling facilities based on CO_2 savings. Finally, Section 6 draws some conclusions.

2. Design method

A two-step optimization procedure is proposed for the conceptual design of A-frame units considering seasonality over a year of operation. The first problem is the optimal design of the geometry for the month with the highest energy production and heat rejection. A detailed model for the A-frame described in Section 3 is used to determine the geometric features of the unit. This model is formulated as an MINLP optimization problem. Section 4.1 shows the tailor-made branch and bound algorithm to determine the number of tubes, number of bundles and rows as well as a standard pipe diameter, tube length and fan blade angle. This problem is solved for the optimal design capable of providing the cooling required.

The seasonal operation of the A-frame over time is addressed for the geometry computed in the design problem. This problem is formulated as a multi-period MINLP to determine the usage of fans, bundles and flow per fan operating on a monthly basis for minimum energy consumption making the most of the unit geometry defined in the first stage. To solve the multiperiod problem the model of the unit is simplified by fixing the geometry. Section 4.2 shows the formulation of the second stage problem. Section 5 reports the main operating data of the case study, heat rejection and weather conditions.

3. Modeling

3.1. CSP facility description

The plant consists of three sections: the heliostat field, including the collector and the molten salts storage tanks, the steam turbine and the air cooler steam condenser. Fig. 1 presents the flowsheet for the process. This process uses a tower to collect the solar energy and a regenerative Rankine cycle. The steam is generated in a system of three heat exchangers where water is heated up to saturation and then evaporated using the total flow of molten salts. However, only a fraction of the flow of salts is used to superheat the steam before it is fed to the first section of the turbine. The rest is used to reheat up the steam before it is fed to the medium pressure turbine. In the medium pressure turbine, part of the steam is extracted and it is used to heat up the condensate. The rest of the steam is finally expanded to an exhaust pressure, condensed and recycled. For the condensation of the steam we propose the use of a direct air cooled system, an A-frame. For the detailed information on the modeling features of the heliostat field and the steam turbine, we refer to previous work [2].

3.2. Air cooling system

A scheme of A-frame type of air condenser can be found in Fig. 2. The exhaust steam from the turbine circulates in a large pipe and it is distributed into the pipes that form a roof over a system of fans in

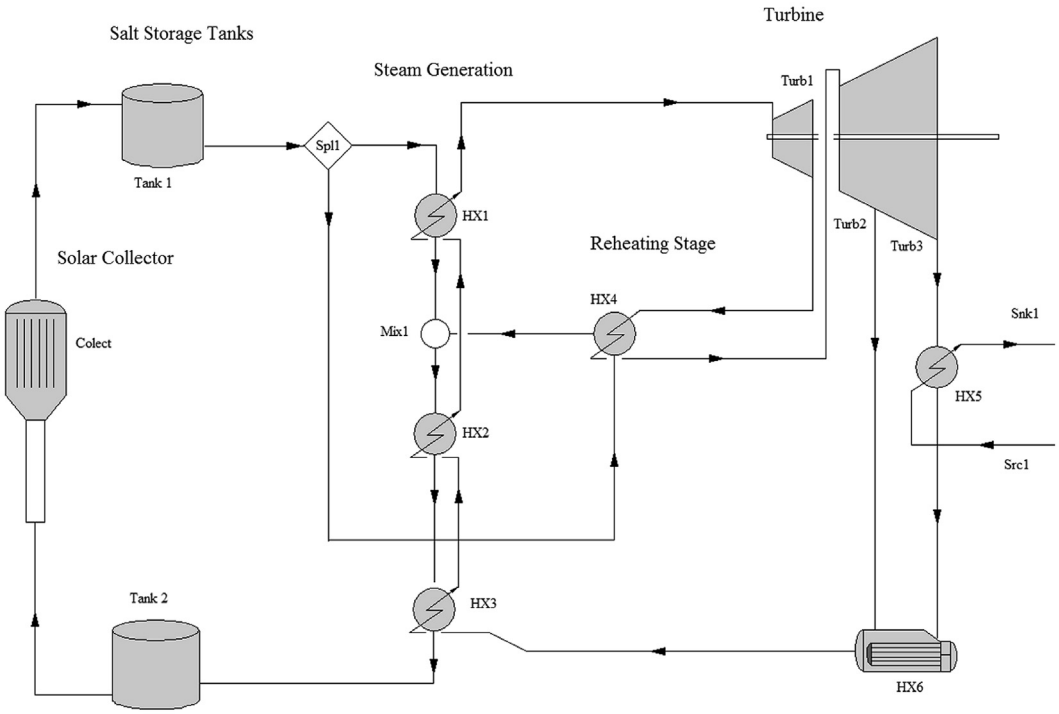

Fig. 1. Flowsheet of the concentrated power plant facility (With permission [11]).

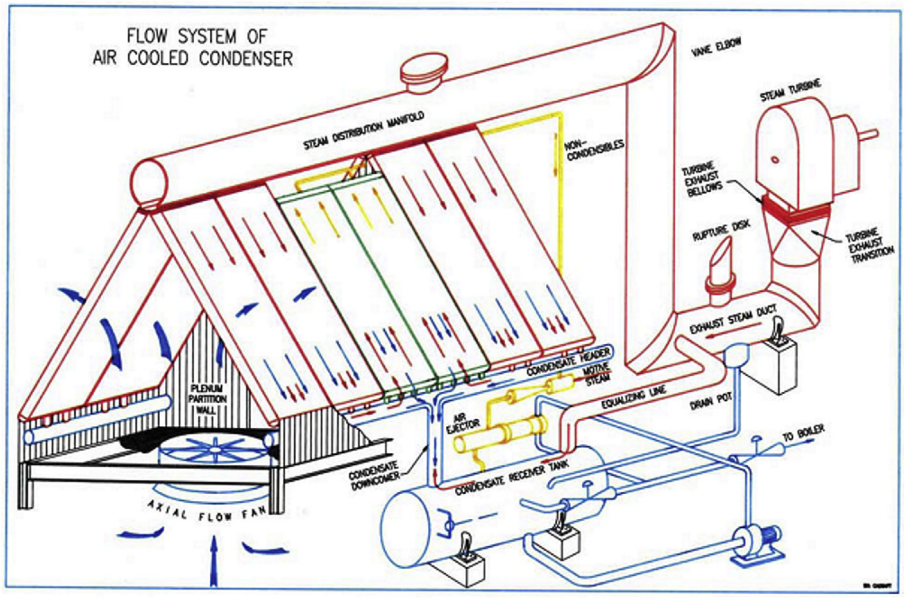

Fig. 2. Scheme of an A-frame type of unit (with permission [19]).

the form of an A. The steam condensers inside the tubes as it descends.

3.3. Model structure

The model is divided in 3 sections: mass and energy balances, A-frame design, and fans design. The mass and energy balances compute the need for air to condense the exhaust steam. Within the A-frame design three main items are evaluated, the heat transfer coefficient, the temperature gradient and the contact area. This area is given by a number of pipes allocated in an inverted V layout, the A-frame. The number of rows of tubes, their length and diameter as well as the number of fins per tube are also calculated. The heat transfer coefficient is highly dependent on the geometry. Internal, external and material resistances are considered to compute the global heat transfer coefficient. Finally, to allow for the air to cross the A-frame structure a certain amount of power is required. It depends on the air flow and the pressure drop generated by the structure. The model is formulated based on first principles, design correlations to estimate heat transfer coefficient,

standard characteristics of pipes and fins [20] and literature data of the operation of the fans. Surrogate models are developed to capture the performance of the fans provided in the form of figures. The heat transfer performance is modelled using widely accepted design equations from the literature. However, if additional fan performance data is available and/or other correlations are developed, the model can be easily updated. The model is optimized for minimum energy consumption.

3.3.1. Mass and energy balances

The two energy balances considered are that to the air flow and the one to the steam. The first of the two determines the air flow required for the operation and is given by Eq. (1):

$$Q = m_{air} \cdot \left[C_{p_{air}} \cdot (T_{out,air} - T_{in,air}) + H \cdot C_{p_{w,vap}} \cdot (T_{out,air} - T_{in,air}) \right] \quad (1)$$

The energy that has to be removed, Q, comes from the energy balance to the steam, as given by Eq. (2) and the data of the operation of the CSP plant [2].

$$Q = m_w \cdot \lambda_w \quad (2)$$

3.3.2. A-frame design

3.3.2.1. Heat exchanger design. The general design equation of any heat exchanger is Eq. (3):

$$Q = U \cdot A_{out} \cdot LMTD \quad (3)$$

This equation has three terms that must be analyzed separately: the logarithmic mean temperature difference, LMTD, the outside contact area, A_{out}, and the global heat transfer coefficient, U.

- **The logarithmic mean temperature difference** LMTD is calculated using Eq. (4):

$$LMTD = \frac{(\Delta T_a - \Delta T_b)}{ln(\Delta T_a / \Delta T_b)} \quad (4)$$

However, eq. (4) is a complex mathematical expression that is typically approximated using Chen approximation within optimization formulations to avoid numerical issues [30], Eq. (5):

$$LMTD \approx \left[\Delta T_a \cdot \Delta T_b \cdot \frac{(\Delta T_a + \Delta T_b)}{2} \right]^{1/3} \quad (5)$$

The temperature's increments ΔT_a and ΔT_b are calculated using Eqs. (6) and (7) where T_v is the steam temperature and $T_{in,air}$ and $T_{out,air}$ the air inlet and outlet temperature:

$$\Delta T_a = T_v - T_{in,air} \quad (6)$$

$$\Delta T_b = T_v - T_{out,air} \quad (7)$$

- **The external contact area of the heat exchanger** A_{out} is the area exposed to the heat flow and it is given by the number of pipes per row and bundle, N_t and N_r, and the number of bundles, N_b, Eq. (8).

$$A_{out} = N_b \cdot N_t \cdot N_r \cdot A_{out,pipe} \quad (8)$$

- **The global heat transfer coefficient** referred to A_{out}, U, can be computed using the equation presented by Pieve and Salvadori [25]. This equation considers the resistances to heat transfer related to steam condensation and the convective heat transfer on the air side; we include also a term that considers the heat transfer resistance due to the conduction of heat across the pipes wall. Thus, U is computed as Eq. (9):

$$\frac{1}{U} = \frac{A_{out}}{\eta_0 \cdot h_{air} \cdot A_{out}} + \frac{e \cdot A_{out}}{k_{mat} \cdot A_k} + \frac{A_{out}}{h_c \cdot A_{in}} \quad (9)$$

We need to compute a large number of variables with remarkable mathematical complexity. The external area efficiency, η_0, is given by Eq. (10) [25]:

$$\eta_0 = 1 - \frac{A_{tf}}{A_{out}} \left(1 - \eta_f \right) \quad (10)$$

where A_{tf} is defined with Eq. (11):

$$A_{tf} = A_f \cdot N_t \cdot N_r \cdot N_b \quad (11)$$

where N_t, N_r and N_b are the number of pipes, the number of rows and the number of bundles respectively. The total fins area, A_f, is computed using the outer fin area $A_{out,fin}$ and Eqs. (12) and (13):

$$A_{out,fin} = \pi \cdot D_f \cdot t_f + \frac{\pi}{2} \cdot \left(D_f^2 - D_{out}^2 \right) \quad (12)$$

$$A_f = n_f \cdot A_{out,fin} \quad (13)$$

The fins efficiency is given by Eq. (14) [25]:

$$\eta_f = \frac{tanh(m\varphi)}{m\varphi} \quad (14)$$

where m and ϕ are calculated using Eqs. (15) and (16) respectively [25] as a function of the pipe geometry, lay out (D_f, D_{out} and t_f) and material (k_f) and the heat transfer coefficient, h_{air}:

$$m = \left(\frac{2 \cdot h_{air}}{k_f \cdot t_f} \right)^{1/2} \quad (15)$$

$$\phi = 0.5 \cdot \left[D_f - D_{out} + t_f \right] \cdot \left(\frac{D_f}{D_{out}} \right)^{\exp[0.065 \cdot m \cdot (D_f - D_{out} + t_f) - 1.3863]} \quad (16)$$

The *air side coefficient*, h_{air}, is calculated using the air Nusselt number. The Nusselt number is defined as presented by Heyns [20] by Eq. (17):

$$Nu = \frac{h_{air} \cdot D_{eq}}{k_{air}} \quad (17)$$

Pieve and Salvadori's equation is used to include the effect of the geometry of the pipes and its lay out (D_f, D_{out}, p_f and t_f) on *Nu*, Eq. (18) [25]:

$$Nu = 0.134 \cdot Re^{0.681} \cdot Pr^{1/3} \cdot \left(\frac{p_f - t_f}{0.5 \cdot \left(D_f - D_{out} \right)} \right)^{0.2} \cdot \left(\frac{p_f - t_f}{t_f} \right)^{0.11} \quad (18)$$

where Reynolds and Prandtl numbers are computed as per Eqs. (19) and (20) [25]:

$$\mathrm{Re} = \frac{\Gamma \cdot D_{eq}}{\mu_{air}} \tag{19}$$

$$\mathrm{Pr} = \frac{\mu_{air} \cdot C_{p_{air}}}{k_{air}} \tag{20}$$

Variable Γ is the airflow across the minimum flow area and the rest are air properties and the equivalent diameter, D_{eq}, for flow purposes. The minimum flow area is computed using Eq. (21) [25]:

$$S_{\min-t} = \left[X_t - D_{out} - \frac{t_f}{p_f} \cdot \left(D_f - D_{out}\right)\right] \cdot L_t \cdot N_t \tag{21}$$

Equation (21) can be used only if equation (22) is satisfied:

$$\frac{X_l}{D_{out}} > 0.5\sqrt{1 + \frac{2X_t}{D_{out}}} \tag{22}$$

However, in this particular case, Eq. (22) is always satisfied because a pipe isosceles triangle layout is selected, see Fig. 3, $X_t = X_l \geq D_{out}$; Thus, Eq. (18) can be used without formulating a disjunction.

The *steam side film coefficient*, h_c, is computed using Eq. (23), as suggested by Heyns [20]:

$$h_c = 0.9245 \cdot \left\{\frac{L_t \cdot \rho_c^2 \cdot k_c^3 \cdot g \cdot \cos(90-\theta) \cdot \lambda_w}{\mu_c \cdot m_{at} \cdot C_{p_{air}} \cdot (T_v - T_{in,air}) \cdot (1 - \exp[-U_c H_t L_t/(m_{at} \cdot C_{p_{air}})])}\right\}^{0.25} \tag{23}$$

where m_{at} and $U_c H_t L_t$ can be computed as per Eqs. (24) and (25) respectively [17]:

$$m_{at} = \frac{m_{air}}{2 \cdot N_t \cdot N_b} \tag{24}$$

$$U_c H_t L_t = \frac{h_{ae} A_a}{2 \cdot N_t \cdot N_b} \tag{25}$$

The $h_{ae}A_a$ term can be computed as follows, Eq. (26) [20]:

$$h_{ae}A_a = k_{air} \cdot \mathrm{Pr}^{0.33} \cdot N_b \cdot A_{fr} \cdot Ny \tag{26}$$

where Ny is computed using Eq. (27) [20]:

$$Ny = 366.007945 \cdot Ry^{0.433256} \tag{27}$$

and Ry by Eq. (28) [17]:

$$Ry = \frac{m_{air}}{\mu_{air} \cdot N_b \cdot A_{fr}} \tag{28}$$

Finally, the *material resistance to the heat transfer* depends on the thermal conductivity of the pipe, k_{mat}. It is estimated as an average for the range of working temperature ranges [31] so that a value of k_{mat} equal to $45 \cdot 10^{-3}$ kJ/(K m^2/m s) is used.

The mean area A_k is computed using Eq. (29):

$$A_k = \frac{(A_{out} - A_{in})}{\ln\left(\frac{A_{out}}{A_{in}}\right)} \tag{29}$$

where A_{in} and A_{out} are calculated as in Eqs. (8) and (30):

$$A_{in} = N_b \cdot N_t \cdot N_r \cdot A_{in,pipe} \tag{30}$$

3.3.2.2. Pipes design for area availability. The pipes are the units that provide the contact area for heat transfer. For an enhanced area, these pipes present fins. The design variables and geometry of pipes are plotted in Fig. 3.

The internal area of a pipe $A_{in,pipe}$ is the area of a cylinder of diameter D_{in} and length L_t. Thus, the area is given as presented in Eq. (31):

$$A_{in,pipe} = \pi \cdot L_t \cdot D_{in} \tag{31}$$

The outside area of a pipe is the sum of fins area A_f and the smooth tube area A_{smooth}, and can be calculated as Eq. (32):

$$A_{out,pipe} = A_f + A_{smooth} \tag{32}$$

where the smooth area is computed by Eq. (33) with is the number of fins per tube length n_{fins} and the mean fin thickness t_f:

$$A_{smooth} = 2 \cdot \pi \cdot \frac{D_{out}}{2} \cdot \left(L_t - t_f \cdot n_f\right) \tag{33}$$

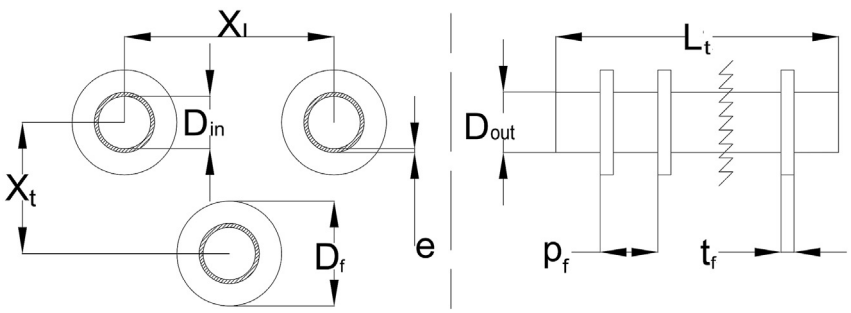

Fig. 3. Geometry of pipes.

The type of fins is selected depending on the kind of fluid which flows in contact with the fins. In the case of the air, a fluid with a small film coefficient and flowing under atmospheric pressure, it is common to employ cross fins [32].

3.3.3. Fans design

The fan is designed so that it generates enough power to overcome the pressure drop across the structure, namely, bundles of tubes, the fan itself and the base of the unit. To model a fan, a detailed characterization is required due to aerodynamic effects of the blade geometry, size, etc. However, such information is not typically available. For this case of study a particular fan has been selected whose charactersitic curves can be found in the literature [24]. This section is divided in two parts: the development of a correlation to predict the power generated by the fan as a function of the flow rate, and the development of models for each one of the contributions to the pressure drop.

3.3.3.1. Power per fan. The power required by the fan is that needed to overcome the pressure drop, and can be obtained from Eq. (34):

$$P_{vent} = n_{fan} \cdot P_F = Q_{air} \cdot \Delta p_e \tag{34}$$

The power per fan depends on the geometry of the blade. For our case, Fig. 4 shows the profile for three blades angles, 14°-18°, due to the lack of further information [24].

A surrogate model is developed based on the typical power curves in the literature, see Fig. 4 to evaluate the power consumption as a function of the air flow. A two-stage fitting procedure is carried out to account for two effects, that of the air velocity and the one related to the blade geometry, in particular, the blade angle A second order polynomial is used to capture the effect of air flow on the power, assuming that there is no power consumed for no air flow rate, Eq. (35). There is typically a base consumption. To account for it, the minimum flowrate for a fan to operate will imposed as a lower bound, to avoid very small flows, and an additional base consumption is added if the fan is working.

$$(P_F)_n = \alpha_n \cdot {V_a}^2 + \beta_n \cdot V_a + \varepsilon_n \tag{35}$$

To capture the effect of the blade geometry, the coefficients α, β and ε are a function of flowrate for each blade angle as seen in Table 1. Next, a correlation between their values and the blade

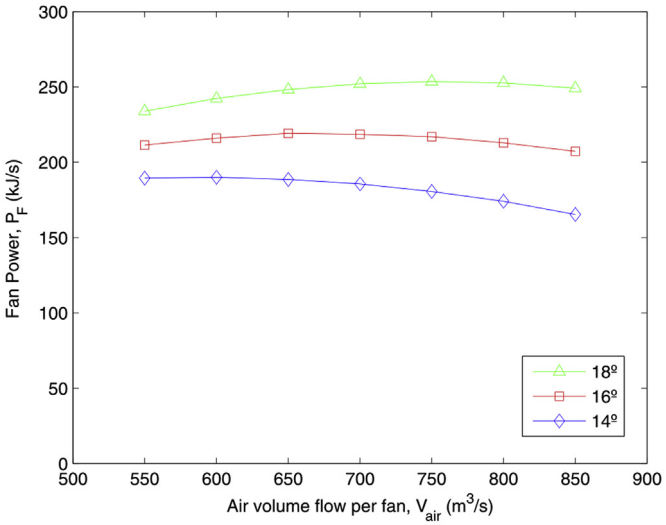

Fig. 4. Experimental data for the fan power.

Table 1
Effect of the blade angle on the power curve.

Angle γ_{pt}	α_n	β_n	ε_n
14	$-4{,}936\,210^{-4}$	$6{,}124\,610^{-1}$	0
16	$-4{,}666\,810^{-4}$	$6{,}396\,310^{-1}$	0
18	$-4{,}411\,310^{-4}$	$6{,}685\,210^{-1}$	0

Table 2
Coefficients for the effect of the angle on the second order polynomial fitting of the power curve.

Coefficient	p	m
α_n	$1.3122 \cdot 10^{-5}$	$-6.7710 \cdot 10^{-4}$
β_n	$1.4015 \cdot 10^{-2}$	$4.1596 \cdot 10^{-1}$
ε_n	0	0

angle is developed, see Eq. (36). It turns out that a linear relationship between coefficients α and β and the angle fits the results. Table 2 shows the parameters:

$$\begin{aligned} \alpha_n &= p_\alpha \cdot \gamma_{bt} + m_\alpha \\ \beta_n &= p_\beta \cdot \gamma_{bt} + m_\beta \end{aligned} \tag{36}$$

Thus, by substituting Eq. (36) into Eq. (35), the expression for P_F becomes Eq. (37):

$$\begin{aligned} P_F = &\left(1.3122 \cdot 10^{-5} \cdot \gamma_{pt} - 6.7710 \cdot 10^{-4}\right) \cdot V_{air}^2 \\ &+ \left(1.4015 \cdot 10^{-2} \cdot \gamma_{pt} + 4.1596 \cdot 10^{-1}\right) \cdot V_{air} \end{aligned} \tag{37}$$

The number of fans is computed as follows, Eq. (38):

$$Q_{air} = n_{fan} \cdot V_{air} \tag{38}$$

3.3.3.2. Pressure drop. The pressure drop across the system is the one responsible for the energy consumed by the fans. To compute it, different contributions such as the pressure drop at the entrance of the structure, before and after the fan and finally through the tubes bundles, apart from the pressure drop across the fan itself are considered, see Eq. (39) [33]:

$$\begin{aligned} \Delta p_e = -\Bigg[&\frac{K_{ts}}{2 \cdot \rho_{a56}} \left(\frac{m_{air}}{N_b \cdot A_{fr}}\right)^2 + \frac{K_{up}}{2 \cdot \rho_{a3}} \left(\frac{m_{air}}{A_e}\right)^2 - \Delta p_{Fs} \\ &+ \frac{K_{do}}{2 \cdot \rho_{a3}} \left(\frac{m_{air}}{A_e}\right)^2 + \frac{K_{\theta t}}{2 \cdot \rho_{a56}} \left(\frac{m_{air}}{N_b \cdot A_{fr}}\right)^2 \Bigg] \end{aligned} \tag{39}$$

Each of the contributions in Eq. (39) require a surrogate model to account for the blade geometry.

- **The fan static pressure**, Δp_{Fs}, is a function of the flow rate and the blade angle, see Fig. 5 developed from the data in Bredell and Kröger [24]. In order to formulate a one equation model to account for both variables, blade angle and air flow rate, the same two-stage procedure as before is used. The mathematical expression that captures the profiles for all all angles is given by eq. (40). Next, the effect of the angles on the coefficients of the master correlation is determined. This correlation will only be valid for the fan whose characteristics have been analyzed. However, the model is flexible and if data for other fans is available, it can be easily updated.

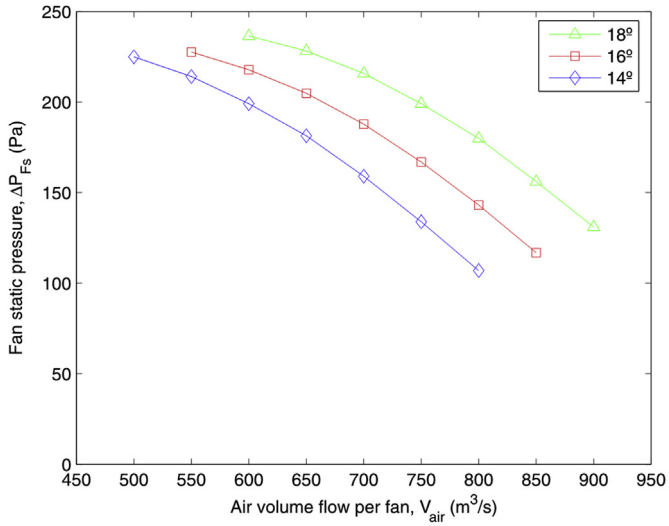

Fig. 5. Experimental fan static pressure.

Table 3
Coefficients of the second order polynomial for static pressure drop.

Blade angle γ_{pt}	α	β	ε
14	$-6.6721\cdot10^{-4}$	$4.7129\cdot10^{-1}$	$1.5645\cdot10^{2}$
16	$-6.8507\cdot10^{-4}$	$5.8780\cdot10^{-1}$	$1.1178\cdot10^{2}$
18	$-6.9630\cdot10^{-4}$	$6.8986\cdot10^{-1}$	$7.3628\cdot10^{1}$

Table 4
Coefficients for the effect of the blades on the static pressure drop.

Coefficient	p	m
α	$-7.2725\cdot10^{-6}$	$-5.6650\cdot10^{-4}$
β	$5.4643\cdot10^{-2}$	$-2.9130\cdot10^{-1}$
ε	$-2.0706\cdot10^{1}$	$4.4524\cdot10^{2}$

$$(\Delta p_{Fs})_n = \alpha_n \cdot V_a^2 + \beta_n \cdot \gamma_{pt} + \varepsilon_n \tag{40}$$

Again, it turns out that a linear regression, Eq. (41), fits the effect of the angle on coefficients α, β and ε of Eq. (40). Only data for 14° –18° are available in the literature to develop this model. Table 3 shows the fitting coefficients of Eq. (40) and Table 4 those of Eq. (41):

$$y = p \cdot \gamma_{pt} + m \tag{41}$$

The extended fitting is provided by Eq. (42):

$$\begin{aligned}\Delta p_{Fs} = &\left(-7.2725\cdot10^{-6}\cdot\gamma_{pt} - 5.6650\cdot10^{-4}\right)\cdot V_{air}^2 \\ &+ \left(5.4643\cdot10^{-2}\cdot\gamma_{pt} - 2.9130\cdot10^{-1}\right)\cdot V_{air} + \Big(\\ &- 2.0706\cdot10^{1}\cdot\gamma_{pt} + 4.4524\cdot10^{2}\Big)\end{aligned} \tag{42}$$

- **Coefficient** K_{ts} represents the pressure drop across fan's support platform, and it is computed using Eq. (43) [34]:

$$K_{ts} = \frac{C_{Dts} L_{ts} d_{ts} n_{ts}}{A_2} \tag{43}$$

The value of C_{Dts} depends on the support beam geometry and the Reynolds number. In this study, it is assumed to be 1.9 [35]. The area A_2 is not well defined because the orientation of the equipment is unknown, thus it is assumed that it corresponds to the rectangular frontal area of the support, Eq. (44):

$$A_2 = 2\cdot\sin(\theta)\cdot L_{ts}\cdot L_t \tag{44}$$

The contribution of the support platform to the pressure drop is corrected by the frontal flow area of an A-frame. It is defined as the area without obstacles in each row of tubes. This area can be calculated using Eq. (45):

$$A_{fr} = \left[N_t\cdot\left(n_f\cdot t_f\right)\cdot\left(X_t - D_f\right) + N_t\cdot(X_t - D_{out})\cdot\left(L_t - n_f\cdot t_f\right)\right]\cdot\sin(\theta) \tag{45}$$

- **Coefficient** K_{up} corresponds to the pressure drop across the obstacles before the fan, such as a protector screen. The value of K_{up} is presented in the literature in the form of figures [34]. A two-step modeling procedure is used to develop a one equation model for K_{up} as a function of the two ratios of variables involved, namely $A_{ob,up}/A_c$ and x_{up}/d_c. The general expression for K_{up} is given by Eq. (46). Table 5 collects the coefficients for various x_{up}/d_c ratios. In this case, the effect of the second variable on the coefficients of Eq. (46) is not linear but is given by Eq. (47) (See Table 6).

$$K_{up} = \alpha_n\cdot\left(\frac{A_{ob,up}}{A_c}\right)^2 + \beta_n\cdot\left(\frac{A_{ob,up}}{A_c}\right) + \gamma_n \tag{46}$$

$$\begin{aligned}\alpha_n &= p_\alpha\cdot\left(\frac{x_{up}}{d_c}\right)^{m_\alpha} \\ \beta_n &= p_\beta\cdot\left(\frac{x_{up}}{d_c}\right)^{m_\beta}\end{aligned} \tag{47}$$

The final expression is as follows, Eq. (48):

$$\begin{aligned}K_{up} = &\ 0.1560\cdot\left(\frac{x_{up}}{d_c}\right)^{-1.5854}\cdot\left(\frac{A_{ob,up}}{A_c}\right)^2 \\ &+ 0.0782\cdot\left(\frac{x_{up}}{d_c}\right)^{-0.9947}\cdot\left(\frac{A_{ob,up}}{A_c}\right)\end{aligned} \tag{48}$$

This contribution to the pressure drop is corrected using the free area across the fan, computed using Eq. (49) [34]:

$$A_e = \frac{\pi}{4}\cdot\left(d_c^2 - d_{fh}^2\right) \tag{49}$$

- **Coefficient** K_{do} corresponds to the pressure drop across the obstacles after the fan, such as the shaft. The value of K_{do} can be

Table 5
Coefficients for correlation eq. (46).

x_{up}/d_c	α	β	γ
0.05	14.7401	1.5868	−0.0001
0.10	6.7789	0.6917	0.0086
0.15	3.9267	0.5045	0.0012
0.20	2.1739	0.4121	−0.0035
0.30	0.9797	0.3280	−0.0059
0.40	0.5746	0.1598	0.0003

Table 6
Coefficients for correlation eq. (47).

Coefficient	p	m
α	0.1560	−1.5854
β	0.0782	−0.9947

Table 7
Fitting parameters for eq. (50).

x_{do}/d_c	α	β	γ
0.05	11.7438	2.9460	−0.0090
0.10	9.3812	1.4274	−0.0023
0.15	3.5998	0.9172	0.0062
0.20	1.0998	0.0811	−0.0017

read in the figures presented by Kröger [34]. Similarly to previous coefficients, a one equation model is developed, Eq. (50), that includes the effect of $A_{ob,do}/A_c$ and x_{do}/d_c, whose relations are given by Eqs. (50) and (51):

$$K_{do} = \alpha_n \cdot \left(\frac{A_{ob,do}}{A_c}\right)^2 + \beta_n \cdot \left(\frac{A_{ob,do}}{A_c}\right) + \gamma_n \tag{50}$$

$$\begin{aligned} \alpha_n &= p_\alpha \cdot \left(\frac{x_{do}}{d_c}\right) + m_\alpha \\ \beta_n &= p_\beta \cdot \left(\frac{x_{do}}{d_c}\right) + m_\beta \end{aligned} \tag{51}$$

Table 7 shows the original fitting parameters for Eq. (50) and Table 8 those that allow including the effect of the x_{do}/d_c ratio into the correlation. Again, it turned out to be a linear relationship as given by eq. (51). Eq. (52) shows the final correlation.

$$\begin{aligned} K_{do} = &\left(-75.4268 \cdot \left(\frac{x_{do}}{d_c}\right) + 15.8845\right) \cdot \left(\frac{A_{ob,do}}{A_c}\right)^2 \\ &+ \left(-18.2098 \cdot \left(\frac{x_{do}}{d_c}\right) + 3.6192\right) \cdot \left(\frac{A_{ob,do}}{A_c}\right) \end{aligned} \tag{52}$$

- **Coefficient** $K_{\theta\tau}$ represents the total pressure drop across the heat exchanger bundle and includes the kinetic energy losses across the heat exchanger. This coefficient can be calculated using Eq. (53) under isothermal flow conditions [33]:

$$K_{\theta t} = K_{he} + \left(\frac{1}{sin(\theta_m)} - 1\right)\left(\frac{1}{sin(\theta_m)} - 1 + 2\sqrt{K_{ci}}\right) + K_{dj} + K_o \tag{53}$$

The function $\sin(\theta_m)$ is approximated by a second order polynomial, within the range of typical θ_m (0-90°), to avoid numerical issues. The polynomial obtained is Eq. (54):

$$\sin(\theta_m) = -1.0293 \cdot 10^{-4} \cdot \theta_m^2 + 2.0845 \cdot 10^{-2} \cdot \theta_m - 2.3441 \cdot 10^{-2} \tag{54}$$

The heat exchanger's pressure drop coefficient for normal isothermal flow, K_{he}, is defined by Heyns [20], eq. (55):

$$K_{he} = 4177.08481 \cdot R_y^{-0.4392686} \tag{55}$$

The mean flow incident angle at the heat exchanger inlet θ_m, is function of the A-frame half apex angle θ [33], Eq. (56):

$$\theta_m = 0.0019 \cdot \theta^2 + 0.9133 \cdot \theta - 3.1558 \tag{56}$$

The heat exchanger entrance contraction loss coefficient for normal flow, K_{ci}, is a function of the ratio of the minimum to free stream flow area through the heat exchanger bundle σ and the ratio of the minimum to free stream flow area at the bundle inlet σ_{21} [33]. These three variables can be calculated with Eq. (57)–(60).

$$K_{ci} = \left(\frac{1 - \frac{1}{\sigma_c}}{\sigma}\right) \tag{57}$$

$$\begin{aligned} \sigma_c = &0.6155417 + 0.04566493 \cdot \sigma_{21} - 0.336651 \cdot \sigma_{21}^2 \\ &+ 0.4082743 \cdot \sigma_{21}^3 + 2.672041 \cdot \sigma_{21}^4 - 5.963169 \cdot \sigma_{21}^5 \\ &+ 3.558944 \cdot \sigma_{21}^6 \end{aligned} \tag{58}$$

$$\sigma_{21} = \frac{\left[X_l \cdot (N_r - 1) + D_f\right] \cdot \left[X_t \cdot (N_r - 1) + D_f\right] - \frac{\pi}{4} \cdot D_f^2 \cdot N_t \cdot N_r}{\left[X_l \cdot (N_r - 1) + D_f\right] \cdot \left[X_t \cdot (N_r - 1) + D_f\right]} \tag{59}$$

$$\sigma = \frac{N_t \cdot \left(X_t - D_f\right) \cdot L_t}{N_t \cdot X_t \cdot L_t} \tag{60}$$

Coefficients K_{dj} and K_o represent the kinetic energy loss at the heat exchanger outlet as a result of turbulent decay of the jet of air [20,33]. Fig. 6 shows the geometry configuration. Thus, K_{dj} can be computed by Eq. (61) while K_o is computed by Eq. (62):

Table 8
Fitting parameters for eq. (51).

Coefficient	p	m
α_n	−75.4268	15.8845
β_n	−18.2098	3.6192
γ_n	0	0

$$K_{dj} = \left[\left\{-2.89188 \cdot \left(\frac{L_w}{L_t}\right) + 2.93291 \cdot \left(\frac{L_w}{L_t}\right)^2\right\} \cdot \left(\frac{L_t}{L_s}\right) \cdot \left(\frac{L_b}{L_s}\right) \cdot \left(\frac{28}{\theta}\right)^{0.4} + \left\{\left(\frac{L_s}{L_b}\right) \cdot \exp\left(2.36987 + 5.8601 \cdot 10^{-2} \cdot \theta - 3.3797 \cdot 10^{-3} \cdot \theta^2\right)\right\}^{0.5} \cdot \left(\frac{L_t}{L_r}\right)\right]^2 \tag{61}$$

$$K_o = \left[\begin{array}{l} \left\{ -2.89188 \cdot \left(\frac{L_w}{L_t}\right) + 2.93291 \cdot \left(\frac{L_w}{L_t}\right)^2 \right\} \cdot \left(\frac{L_s}{L_b}\right)^3 + 1.9874 + \\ -3.02783 \cdot \left(\frac{d_s}{2 \cdot L_b}\right) + 2.0187 \cdot \left(\frac{d_s}{2 \cdot L_b}\right)^2 \end{array} \right] \cdot \left(\frac{L_t}{L_s}\right)^2 \quad (62)$$

The rest of the geometry features of the A-frame are computed using Eqs. (63–66):

$$N_{Lr} = \frac{L_w}{cos(90 - \theta)} \quad (63)$$

$$L_r = N_{Lr} + L_t \quad (64)$$

$$L_b = L_r \cdot cos(90 - \theta) \quad (65)$$

$$L_s = \left(\frac{d_s}{2} + L_r\right) \cdot sin(\theta) - \frac{d_s}{2} \quad (66)$$

Furthermore, the bounds for the size of the fan are as follows, Eqs. (67)–(69), so that the fan can be allocated below the A-frame:

$$d_c \leq 2 \cdot \sin(\theta) \cdot L_t \quad (67)$$

$$n_{fan} \cdot d_c + Sep_{fan} \cdot \left(n_{fan} - 1\right) \leq X_t \cdot N_t \quad (68)$$

$$n_{fan} \cdot \frac{\pi}{4} \cdot d_c^2 + Sep_{fan} \cdot \left(n_{fan} - 1\right) \cdot 2 \cdot \sin(\theta) \cdot L_t \leq \frac{\pi}{4} \cdot 2 \cdot \sin(\theta) \cdot L_t \cdot \frac{N_b}{2} X_t \cdot N_t \quad (69)$$

The distance of upstream obstacles x_{up} and the distance of downstream obstacles x_{do} have to satisfy the following constraints, Eqs. (70)–(73) [34]:

$$x_{up} \geq 0.05 \cdot d_c \quad (70)$$

$$x_{up} \leq 0.40 \cdot d_c \quad (71)$$

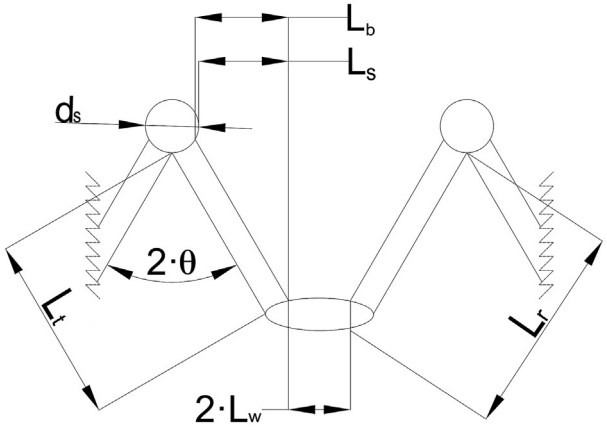

Fig. 6. Pipe configuration.

$$x_{ab} \geq 0.20 \cdot d_c \quad (72)$$

$$x_{do} \leq 0.20 \cdot d_c \quad (73)$$

3.4. -Ranges for variables and parameters

The ranges for the design variables are defined using the data from the literature to ensure representative solutions. These value ranges are collected in the supplementary material based on data from the literature for the pipes and the bundle, Table S1 [11,19,20,24,33], the characteristics of the fan in Table S2 [11,24,30], and the support geometry in Table S3 [36,37].

Some variables, i.e. fan diameter, are fixed based on data from the literature in order to solve it. However, these values can be replaced by variables if there exists information to build models that correlate them to the power consumption, etc. Some geometric variables are fixed based on typical standard values:

- The fan's specifications are defined by the manufacturer [24]. See Table S4 in the supplementary material.
- Some specifications of the bundles are fixed as seen in the supplementary material, Table S5. In this case, we used the following assumptions:

- The pipe thickness is the standard value to the minimum inner pipe diameter [38]. This value has to be modified if the diameter takes distant values from the minimum inner diameter.
- The fin thickness, t_f, is fixed [11].
- The inner diameter of the steam pipe is fixed according to the maximum annual steam flow, the steam flow of the month July. In this case, the value of d_s is the same as Heyns [20].
- According to the small size of the facility of our case study, L_w takes the value of 0, because the tube bundles are distributed in a single street of bundles.

4. Optimization procedure

The link between design and seasonal operation is evaluated by proposing a two-step optimization procedure. The detailed model presented in Section 3 cannot be used to evaluate the seasonal performance and a simplified model is developed based on the detailed design. This section is divided into two. Section 4.1 shows the objective function used to design the A-frame. Finally, Section 4.2 shows the model used to evaluate the operation of the plant over time.

4.1. Optimal equipment design

The model formulated in Section 3.3, an MINLP, is solved by using a tailor-made Branch and Bound method for the month of the largest cooling load. The objective function is based on the annualized cost of the unit including the cost of operation. The estimation of the cost of the units is based on the equipment cost to

compute the facility investment cost, and the power consumed to run it, as the operating cost. The equipment cost can be divided into fan cost and A-frame heat exchanger cost. The equipment cost can be estimated using Eqs. (74)–(76) [26,42]:

$$C_{frame} = 3109 \cdot A^{0.40} \tag{74}$$

$$C_{fan} = K_2 \cdot 2.2 \cdot [1 + 0.2164 \cdot \ln(\Delta p_e)] \tag{75}$$

$$K_2 = 10^{2.9471 + 0.3302 \cdot \log_{10}(v_{std}) + 0.1969 \cdot \log_{10}(v_{std})^2} \tag{76}$$

The monthly amortization, Eq. (77), is determined considering that the expected life of the A-frame bundles is 25 years [19], while the fans lifespan is considered to be 18 years [43].:

$$Amort_{equipment} = \frac{C_{equipment}}{12 \cdot DeLi_{equipment}} \tag{77}$$

The cost for the power consumed is estimated using Eq. (78):

$$C_{elec} = \frac{1}{\eta_{fan}} \cdot P_F \cdot \left(744 \frac{kWh \cdot s}{kJ \cdot month}\right) \cdot C_{\$-kWh} \tag{78}$$

Thus, the objective function for the problem described in Section 3.3 becomes, Eq. (79):

$$Z = Amort_{frame} + Amort_{fan} + C_{elec} \tag{79}$$

The solution procedure is as follows. A deep first approach is implemented. The branching starts on the number of rows N_r, next the number of tubes per row N_t, subsequently the number of bundles of tubes, N_b. At this point the D_f is used as lower bound for X_t and X_l. The next level of the tree corresponds to the inner diameter and the outer diameter of the tube D_{in} and D_{out}. Subsequently, the tube length L_t is fixed using intervals of 0.15 m [44]. At this point the number of fins per tube length is already fixed, n_f, and the fins diameter D_f. Finally, the number of fans n_{fan} is computed.

Each relaxed NLP problem at any node is solved using a multi-

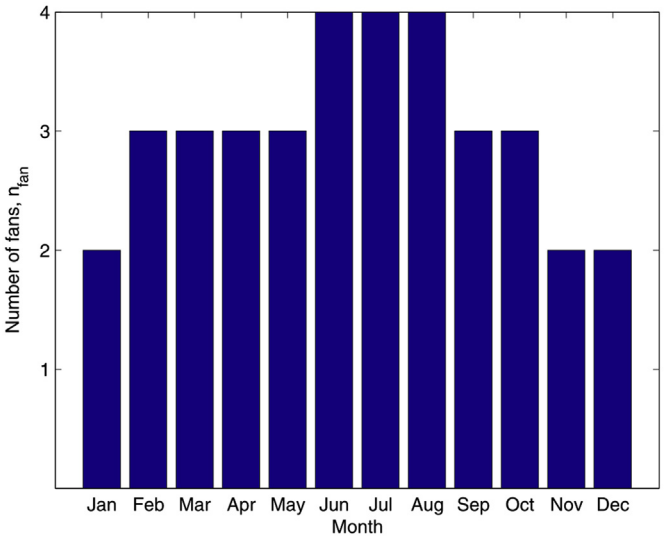

Fig. 8. Use of fans over the year.

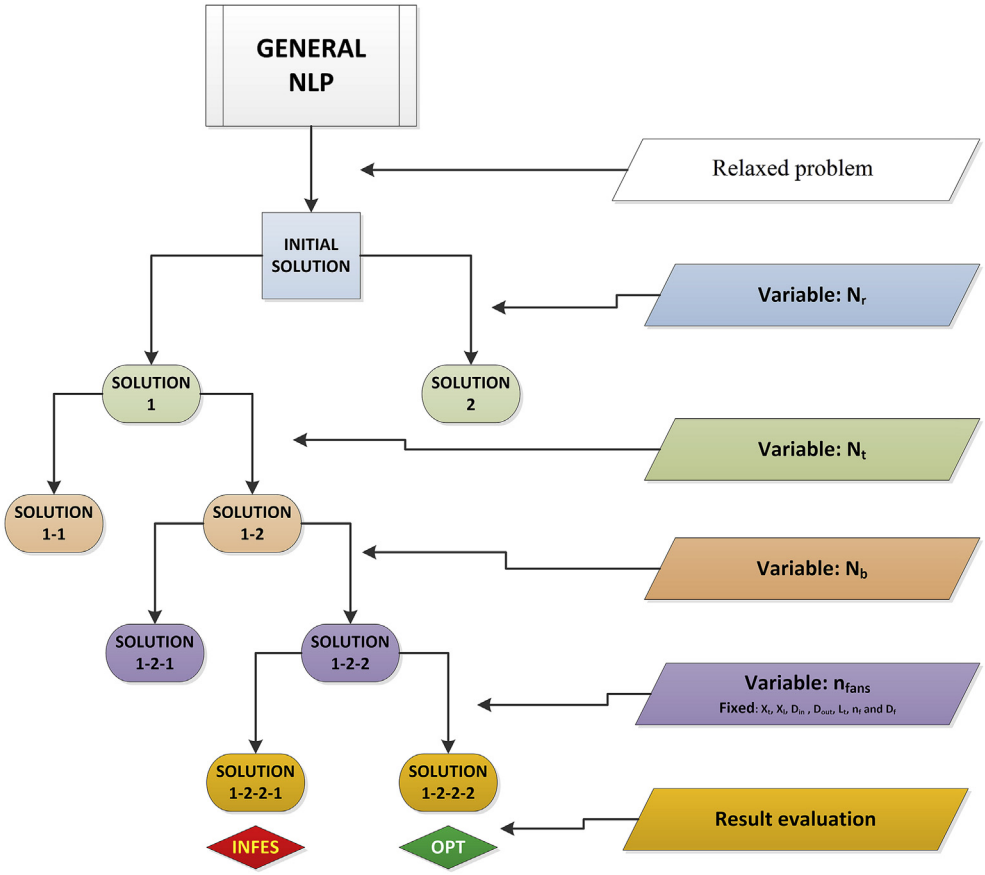

Fig. 7. Branch and Bound tree.

start initialization procedure. The problem size is about 150 eqs. and similar number of variables. It is also possible that some decision variables can be fixed at the same node because their values are at integer values already, typically at the bounds. In each step of the procedure the objective function is compared to the other solutions of the branch and bound tree to decide how to continue. The resulting decision tree for this case can be seen in Fig. 7 below.

4.2. Optimal operating conditions

The optimal geometric design provided by the previous problem is applied to study the unit operating conditions on a monthly basis. This part of the problem works as a recourse. The evaluation of monthly operating conditions is carried out by formulating a multi-period optimization model aiming at minimum the energy consumption over an entire year once the geometry is fixed. Hourly level operation is not considered a design but a control problem and it is not addressed in this work. However, for such a model to be solved, the highly non-linear equations of the design model must be simplified. First, all variables related to the mechanical design of the equipment (pipes, bundles, fans and support structure's specifications) are fixed using the results of the optimal design. Then, the coefficients that depend on those variables (K_{up}, K_{do} and K_{ts}) are computed and fixed. Air thermodynamic properties are also fixed to average annual values since there is not much variation throughout the year. Next, the rest of the variables are transformed into monthly depended parameters or variables. For instance, the heat transfer coefficients are simplified considering an average global heat transfer coefficient, U, for each month (m). The values of U are obtained optimizing the operating conditions for each month individually. Tables 9 and 10 present the main operating and atmospheric conditions. Thus, the heat coefficient U becomes $U \rightarrow U(m)$. Table 11 shows the values of U.

Similarly, other variables are also made monthly dependent: $A_{out}(m)$, $Q(m)$ $LMTD(m)$, $\Delta T_a(m)$, $\Delta T_b(m)$, $T_{out,air}(m)$, $T_{in,air}(m)$, $m_{air}(m)$, $m_w(m)$ and $Q_{air}(m)$. These variables cannot be fixed because the area required, the air flow and the energy balances change on a monthly basis.

Finally, the multi-period model involves the energy balances, the design equation for the heat exchanger and a set of equations grouped into four blocks as follows:

- **Global equations**: eqs. (80) and (81):

$$n_b^{tot}(m) = \sum_{i=1}^{n_{fan}} n_b^i(m) \tag{80}$$

$$Q_{air}(m) = \sum_{i=1}^{n_{fan}} V_{air}^i(m) \tag{81}$$

- **Fans equations**: eqs. (82)–(85):

$$V_{air}^i(m) \le f^i(m) \cdot 700 \tag{82}$$

$$V_{air}^i(m) \ge f^i(m) \cdot 50 \tag{83}$$

$$f^i(m) \cdot b_{fan}(m) \ge n_b^i(m) \tag{84}$$

$$n_{fan}(m) = \sum_{i=1}^{n_{fan}} f^i(m) \tag{85}$$

Variable b_{fan} is defined considering that, after the design of the equipment, the pipes bundles will be distributed equitably among the fans.

- **Power equation**: eqs. (86)–(88):

$$P_{vent}(m) = \sum_{i=1}^{n_{fan}} P_F^i(m) \tag{86}$$

$$\begin{aligned} \Delta p_e^i(m) &= \Delta p_{Fs}^i(m) + 4.5922 \cdot 10^{-8} \cdot \left(m_{fan}^i(m)\right)^2 \\ &+ 4.5922 \cdot 10^{-8} \cdot \left(m_{fan}^i(m)\right)^2 + 9.38925 \cdot 10^{-6} \cdot \left(m_{fan}^i(m)\right)^2 \\ &+ 1.1207 \cdot 10^{-5} \cdot \left(m_{fan}^i(m)\right)^2 + \left(-6.2129 \cdot 10^{-8} \cdot V_{air}^i(m) \right. \\ &\left. + 1.3642 \cdot 10^{-4}\right) \cdot \left(m_{fan}^i(m)\right)^2 \end{aligned} \tag{87}$$

$$P_{vent}(m) = \sum_{i=1}^{n_{fan}} \left(\Delta p_e^i(m) \cdot m_{fan}^i(m)\right) \tag{88}$$

- **Redefined equations**: Eqs. (8) and (30) are redefined using the variable n_b in order to calculate $A_{in}(m)$ and $A_{out}(m)$:

$$A_{in}(m) = n_b^{tot}(m) \cdot N_t \cdot N_r \cdot A_{in,pipe} \tag{8 *}$$

$$A_{out}(m) = n_b^{tot}(m) \cdot N_t \cdot N_r \cdot A_{out,pipe} \tag{30 *}$$

- **The objective function** is given by Eq. (89) aiming at the minimum annual consumption of energy Eq. (89). A base of 20 kW is assumed as the power required to switch on a fan:

Table 9
Atmospheric conditions [39–41].

MONTH	kWh/m²·day	Day	SUN (H)	Sun (h/day)	$T_{in,air}$ (°C)	% Humidity
J	4.377	31	191	6.161	12.5	69
F	5.125	28	191	6.821	13.2	68
M	5.319	31	228	7.355	14.7	66
A	6.387	30	250	8.333	16.4	64
May	6.697	31	299	9.645	19.1	66
June	8.587	30	322	10.733	22.7	64
July	8.668	31	338	10.903	25.7	63
Aug	7.342	31	312	10.065	26.4	65
Sep	6.057	30	257	8.567	24.0	66
Oct	4.126	31	221	7.129	20.0	68
Nov	3.513	30	187	6.233	16.2	70
Dec	3.326	31	176	5.677	13.7	70
Average	5.794	30.4	248	8.13	18.7	66.6

Table 10
Monthly operation of the CSP plant [2].

	Jan	Feb	Mar	Apr	May	Jun	Jul	Aug	Sep	Oct	Nov	Dec
Q**(kW)**	18 650	21 610	22 460	27 120	28 400	36 450	36 870	30 940	25 850	17 380	14 830	13 990
$T_{in,air}$**(°C)**	12.5	13.2	14.7	16.4	19.1	22.7	25.7	26.4	24.0	20.0	16.2	13.7
T_v**(°C)**	59.7	59.7	59.7	59.7	59.7	59.7	59.7	59.7	59.7	59.7	59.7	59.7
P_{gen}**(kW)**	12 623	14 632	15 206	18 362	19 222	24 673	24 959	20 943	17 201	11 763	10 042	9468

Table 11
U values per month.

Month	U (J/K m^2 s)
Jan	444
Feb	465
Mar	473
Apr	500
May	512
Jun	546
Jul	573
Aug	541
Sep	517
Oct	458
Nov	426
Dec	412

$$Z = \sum_{m=1}^{12} \sum_{i=1}^{n_{fan}} \left(P_F^i(m) + 20000 \cdot f^i(m) \right) \tag{89}$$

The problem size is 529 equations, 481 continuous and 120 discrete variables. Note that control is out of the scope of this paper.

5. Results

The case study of the Concentrated Solar Power facility developed in Martín and Martín [2] is used. This facility is based on an actual one in Spain. It is a small facility producing around 20 MW a year, located in a region where solar incidence is high and the availability of water is becoming a challenge. The results section is divided into four parts. After describing the case of study, the geometric design of the unit for the month of the largest cooling load is presented. A sensitivity analysis evaluating the effect of the cost of electricity and the fan performance is carried out. Next, for a fixed geometry, the operation over a year is optimized. Finally, the economics and CO_2 emissions of dry and wet cooling systems are evaluated.

Table 12
Optimal design for July.

Variable	Values n° 1	Values n° 2
θ (°)	62.93	62.93
L_t (m)	13.50	13.50
D_{out} (m)	0.033	0.033
D_{in} (m)	0.027	0.027
D_{eq} (m)	0.033	0.033
N_t	75	75
N_r	1	1
N_b	16	16
D_f (m)	0.043	0.043
n_f	34.351	34.347
Fins per pipe	464	464
X_t (m)	0.15	0.15
X_l (m)	0.15	0.15
n_{fan}	4	4
b_{fan}	4	4
γ_{pt} (°)	16.38	16.38
L_{ts} (m)	9.47	6.00
d_{ts} (m)	0.10	0.10
x_{up} (m)	0.60	0.60
x_{do} (m)	1.50	1.50
C_{frame} ($)	175,055	175 073
C_{fan} ($)	1,651,070	1651 070
C_{elec} ($/month)	77,476	77,470
Z ($/month)	**85703.36**	**85697.42**

5.1. Operating data

The facility is located in the same region as the one in the work by Martín & Martín [2]. The operating conditions, weather data and plant operation are collected in Tables 9 and 10:

5.2. Equipment design

The Branch and Bound tree that leads to the solution is plotted in Fig. 7. Solution 1 had a value of the objective function Z equal to 84 958.09 $/month, and the Solution 2 of 107 366.80 $/month, thus the Solution 2 node was phantomed. At the second level, the Solution 1-1 had Z = 85 124.38 $/month and the Solution 1–2 Z = 84 958.09 $/month, thus the Solution 1-1 node was phantomed. Checking the solutions of the third level, it is noted that Solution 1-2-1, Z = 86 211.34 $/month, and Solution 1-2-2, Z = 85 659.96 $/month, suggest that the Solution 1-2-1 node to be phantomed. At the last level, Solution 1-2-2-1 was infeasible, thus the optimal solution for the case of study was Solution 1-2-2-2. The optimal design for the equipment is collected in the column labeled as *Values n°1* on Table 12.

The equivalent diameter was the same as D_{out}, which is due to the fact that the tubes only have a small number of fines. Using this result, the model is solved assuming $D_{eq} \approx D_{out}$. The results are shown on the column labeled as *Values n°2* on Table 12. The results presented in Table 12 are very similar. However, L_{ts} takes a different value in both solutions. The main reason for this difference is the fact that the variable is loosely bounded. Nevertheless, the values of variables L_{ts} and d_{ts} need to be checked based on mechanical considerations of the support structure. The optimal apex angle is 62.93°, which is within the typical range. Most of the units are designed with an apex of 60° which was already obtained in the literature [27]. This result differs from typical air coolers where the pipes are horizontal [26]. Note that the model allowed that possibility, but the results showed otherwise. n_f turned out to be 34.35 and the total number of fins per tube turned out to be 464; both values show that finned tubes are needed to provide enough transfer area, although the value of n_f is smaller than fully finned tubes as used previously. Fins increase the pressure drop at the cost of providing a larger contact area. As a result, the system tries to reduce the pressure drop and increases the number of tubes [24]. The value of n_f is small because there is no limit to the ground footprint of the units, and this is the option with the smallest pressure drop. Even though, the value is a tenth compared to the values in the literature, 393.7 fines per m [26]. A constraint about layout availability will modify the result, thus some variables as X_t, N_t or N_r could change since all the pipes needed are arranged in the same row and even the number of fins per unit length if more area

Table 13
Effect of electricity price on the design.

Variable	Original	Original	E_{cost} +20%	E_{cost} −20%	η = 40%	η = 90%
η	60	60	60	60	40	90
θ (°)	62.93	62.93	62.93	62.93	62.92	62.92
L_t (m)	13.50	13.50	13.50	13.50	13.50	13.50
D_{out} (m)	0.033	0.033	0.033	0.033	0.033	0.033
D_{in} (m)	0.027	0.027	0.027	0.027	0.027	0.027
D_{eq} (m)	0.033	0.033	0.033	0.033	0.033	0.033
N_t	75	75	75	75	75	75
N_r	1	1	1	1	1	1
N_b	16	16	16	16	16	16
D_f (m)	0.043	0.043	0.043	0.043	0.043	0.043
n_f	34.351	34.347	34.347	34.307	34.449	34.449
Fins per pipe	464	464	464	463	465	465
X_t (m)	0.15	0.15	0.15	0.15	0.15	0.15
X_l (m)	0.15	0.15	0.15	0.15	0.15	0.15
n_{fan}	4	4	4	4	4	4
b_{fan}	4	4	4	4	4	4
γ_{pt} (°)	16.38	16.38	16.38	16.38	16.38	16.38
L_{ts} (m)	9.47	6.00	9.47	8.68	7.93	9.47
d_{ts} (m)	0.10	0.10	0.10	0.10	0.10	0.10
x_{up} (m)	0.60	0.60	0.60	0.60	0.60	0.60
x_{do} (m)	1.50	1.50	1.50	1.50	1.50	1.50

is required. For instance, typically the number of rows of pipes is 2 [25,27] or 4 [26] even though this last design is not an A-Frame but the pipes are horizontal. The use of multiple rows increases the pressure drop and is meant to provide a larger heat transfer surface per cross sectional area. To reduce power consumption a single row of pipes is suggested. Furthermore, the number of tubes per row is also smaller, around 60 [25], or 56 for the horizontal design [26] and shorter tubes were installed, around 9 m [34] or 10.9 m [26] versus 13.5 *m*, See Table 12. The A-frame layout results in larger pipes compared to the design in Ref. [26]. Another interesting comparison is that the diameter of the tube obtained in previous work is 3.68 mm [27] while our results suggest smaller diameter, 3.3 mm. This fact results in larger heat transfer coefficients reducing the need for contact area. Finally the pitch distances are larger than the one in other designs [26,27], to reduce the pressure drop. Even though the design resulting from the optimization cannot be validated with a physical unit, the results obtained agree with the designs in the literature [24–27,34].

One of the variables with larger uncertainty is the electricity

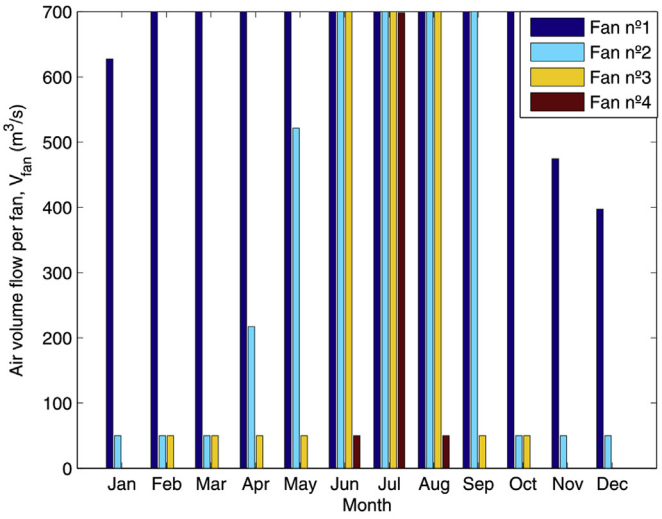

Fig. 10. Air volume flow rate used per fan and month.

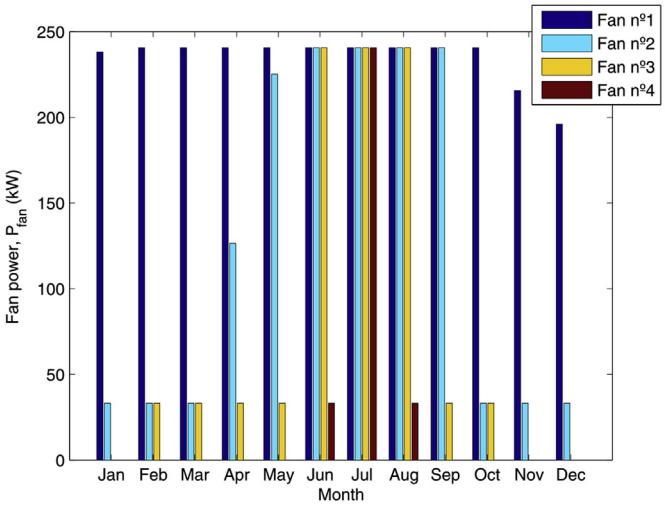

Fig. 11. Power used per fan and month.

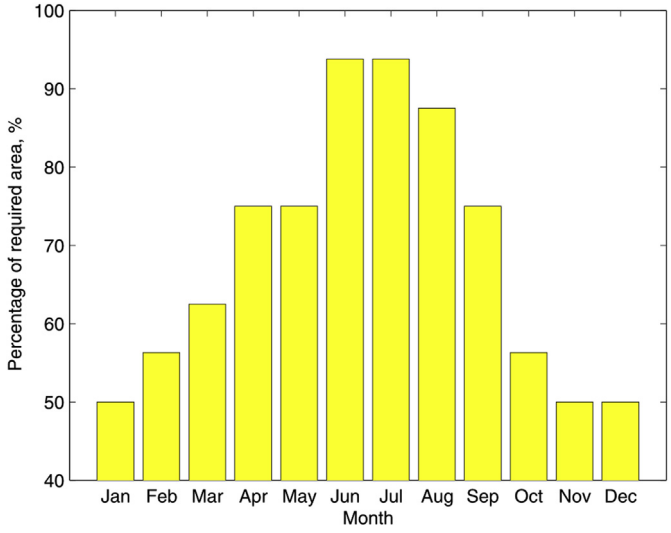

Fig. 9. Area used per month.

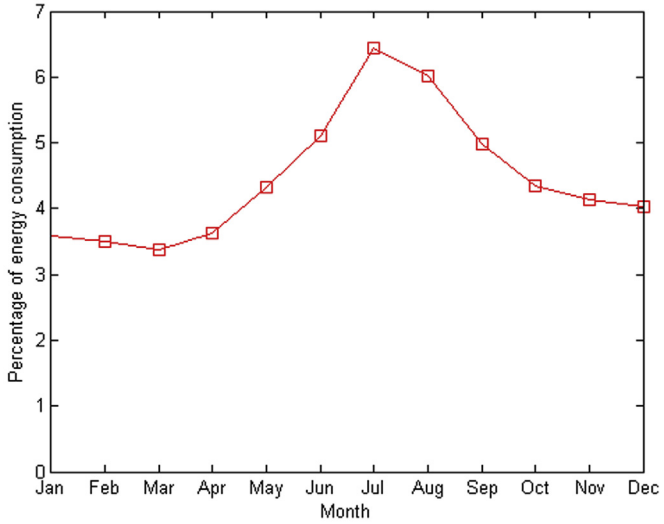

Fig. 12. Percentage of Energy consumption.

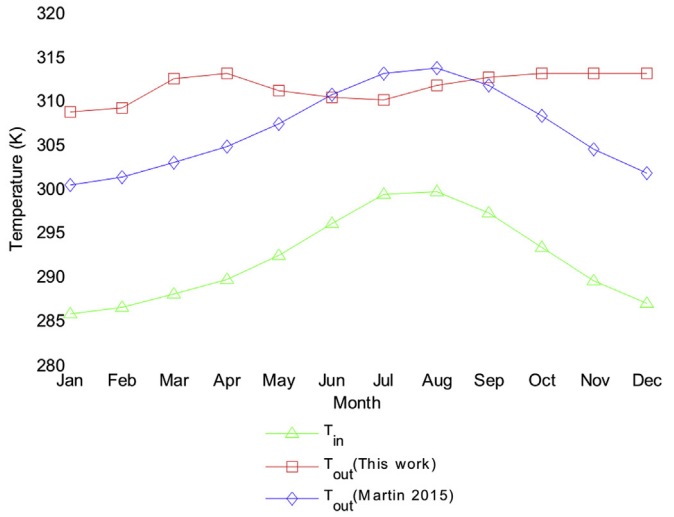

Fig. 13. Temperature gradient across the unit.

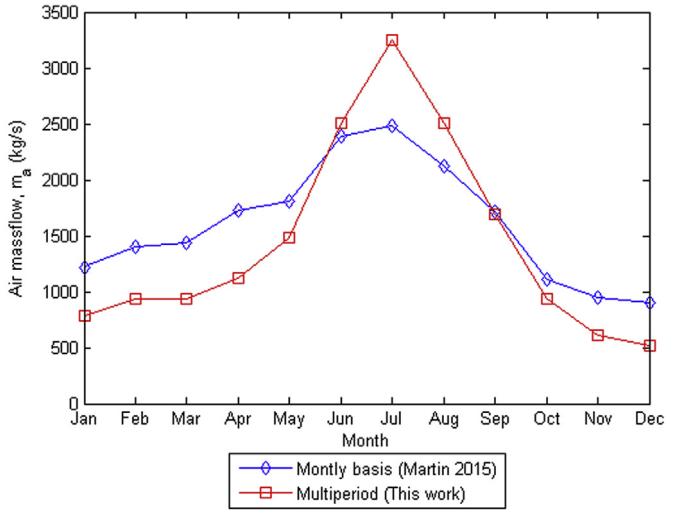

Fig. 14. Total mass flowrate used per month (Multiperiod, squares; Montly basis, triangles).

cost, the second one is the fan performance. A sensitivity analysis is performed using a range of values from −20% to +20% of the original value were used. The results of the optimal design, following Section 4.1, are almost the same as those in Table 12, see Table 13. Slight differences can be found in one variable that is not tightly constrained and therefore the model has more freedom to select the final value such as L_{ts}. Even though, the result is close, 8.47 *m*–9.74 *m*. The rest values, but for the number of fines per pipe, are the same. In this case, the more common value obtained is 464 fines per pipe, but in the case of using an electricity cost 20% lower than the base case. However, the actual difference, 464 vs. 463, can be due to numerical issues. The second variable analyzed is the fan performance. The base case uses a value of 60% based on the literature [24]. In Table 13 the main characteristics of the A-frame are presented. Again, the only difference corresponds to the length of the support of the A-frame, L_{ts}, that is reduced to 7.93 *m* in case the performance is 40%. The fins per pipe are 465 instead of 464, that can be due to numerical issues more that an actual difference. Evaluating the results in Table 13 it is possible to conclude that the design is rather robust.

5.3. Operation

For the optimal geometry of the unit defined in the previous stage, we optimize the operation of the system for minimum power consumption. This problem becomes a multi-period MINLP optimization one. It can be considered as a recourse where, it is up to the operation to decide the number of fans used, the outlet air temperature and the flow used per fan. It is assumed that for a fan to operate, a minimum flow rate of 50 m^3/s is required. Figs. 8–14 show the results obtained. In Fig. 8 it can be seen that the fans are fully used during summer, June to August. During winter, a fourth of the year, only half of the units are needed. The reason is that the CSP facility is producing less than haft power than in winter and, in consequence, rejecting also less heat. As a result, assuming that it is possible to shut down some sections of bundles for better efficiency so that a decrease in the heat transfer coefficient due to low flow rates is avoided, Fig. 9 presents the actual area needed on a monthly basis. Again, winter time requires only half of the system available area, while during summer time there still exists a small margin of operation of about 5%. This margin is interesting for flexibility purposes. From the economic point of view, the investment in the A-frame is only fully used a quarter of the entire year, while the rest the units are underused, which is one the burdens for the operation of these plants. For half a year the area used is lower than 75% of that available. So far, the high costs of the solar field, representing almost 60% of the investment in units [2] mitigates the economic impact for under usage of the heat exchanger network of the plant the turbine and the cooling system. However, the solar field is the one that is currently improving its efficiency since the rest of the process is similar to current thermal power plants, therefore it is expected that idle units will show a larger contribution to the investment in the near future.

The monthly operation also depends on the air flow used per fan and month. In principle, it is only when a fan is fully used when the second one enters in operation. However, that is not exactly correct in all cases. Sometimes, when only a small extra need is required from another fan, it is more efficient to use two fans at a lower flowrate, rather than only one using a larger flow, see Fig. 10. A minimum flow of 50 m^3/s is set for a second fan to operate. As a result of the economics, even if it would be possible to meet the cooling needs with one fan, every single month uses at least two fans, with one of them operating at the minimum load allowed. In January the first fan is operating close to its full capacity, around 625 m^3/s, so there is still margin to accommodate the rest of the air processes. November and December show a different behavior. In these two months a little over a half of the capacity of the first fan, 470 and 400 m^3/s, is used and yet a second one is in operation. It is possible to see that only July requires the full use of the 4 fans, while June and August have three fans operating at full capacity and the fourth one at the minimum. Similarly, for April and May a third fan is operating even though there is enough cooling capacity with two. The second fan in April is at one third of its full capacity while the second fan for May reaches three fourths of its full capacity. This can also be due to the shape of the pressure drop curve as a function of the flow rate as well as the minimum air flow across a fan required for it to operate. Fig. 11 is similar to Fig. 10 where instead of presenting the air flow rate, power is shown. Around 1 MW of cooling power is needed during July compared to a little over 250 kW during winter.

The aim of this work is to reduce the energy consumption of dry cooling systems. The efficiency of the system is given by the fraction of the total energy produced by the CSP facility that needs to be diverted to the cooling system. Assuming that the fans have an efficiency of $\eta_{fan} = 60\%$ [24], Fig. 12 shows the percentage of energy

consumed by the fans. We see that it is not constant over the year but there is a peak during summer, and in particular, in July. Note that the maximum power consumption takes place during that month, and that there is no proportionality between the power produced by the CSP facility and the power consumed by the cooling system. The A-frame system consumes from 3% in winter to 6.5% in August. This variation can be justified combining the information related to the fans operation in Figs. 10 and 11 with the one provided in Fig. 13. The cooler the temperature, the larger the driving force for heat transfer reducing the area needed and the pressure drop. Fig. 13 shows that the air temperature exiting the A-frame system is almost constant resulting in large temperature gradients of up to 25 K in winter, but a reduced 10 K in summer. As a result, the heat transfer area required in summer is not only due to the heat rejection, but also due to the reduced temperature gradient. Furthermore, in Fig. 14 it is possible to see that the air flow rate follows a profile similar to the one of the fraction of energy consumed, given by Fig. 12. There is a large increase in the mass flow rate used in June to August resulting in the need for the use of 4 fans to move that amount of air. Again, the reason is the need for larger contact areas due to a reduced heat transfer driving force. Furthermore, Fig. 13 also shows that if the system is optimized on a monthly basis, the ΔT is maintained constant over the months [11]; however, the multi-period optimization suggests using as much temperature difference as possible every single month, see Fig. 13, so that for most of the year the total mass flow rate used is smaller. As a result, the power required to move it also decreases compared to the standalone monthly operation. This is a particularly interesting result obtained by the multi-period optimization since it proves that the optimal operation of the units that use solar energy cannot be efficiently carried out on a monthly basis or using a scenario based approach but a full year of operation must be considered. The use of a multiperiod approach makes the most of the resources available reducing the operating costs. This result also supports the use of the approach presented in this work.

The comparison ot these results with the ones in the literature is not straightforward. In previous works a fan efficiency of 90%, $\eta_{fan} = 90\%$,was used. To compare the results of this work with the numbers presented in the previous one [11], the same fan efficiency must be considered. Using this efficiency, the energy consumption turns out to be 4.3%. The optimization of the unit allows reducing the energy consumption by 0.7% of the power produced by the facility corresponding to 10–20% savings with respecto to other models and the literature. Note that the design provided by this work is a detailed one, unlike the one in Ref. [11] where the entire facility is considered. Fig. 15 shows the comparison between the power consumed by the fan in previous work [11] and that presented in this work considering $\eta_{fan} = 90\%$. During summer time, 20% savings are reported but for winter-spring time, almost half of the energy is saved.

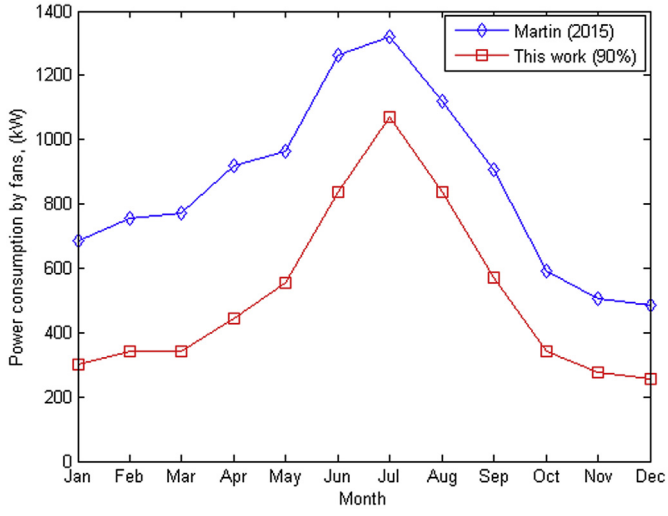

Fig. 15. Comparison of the multiperiod optimization and the montly basis operation.

The variability in solar incidence and weather conditions constitutes a scheduling and control problem to be addressed at a more detailed time grid for the use of variable sources of energy. These issues will be addressed as future work by extending the model to deal with uncertain weather conditions at hourly or subhourly level, taking into account that they will also affect the operation of the plant that this cooling system serves and therefore an integrated solution is to be provided.

5.4. Economic and environmental evaluation

The assessment of A-frame systems is performed comparing the cost and emissions of the A-frame with those of a wet cooling tower.

1 The economic evaluation is divided into two parts: equipment cost and monthly operating cost.

The equipment cost of the A-frame, involving bundles and fans, is estimated using eqs. (74)–(76), while eq. (90) is used to estimate the cost of the cooling tower [45]. In this case, a value of 800 m^3/s is considered for the variable v_{std} in order to take into account a fan with the manufacturer's characteristics.

$$C_{tower} = 101923 \cdot \left(Q \cdot 3.414 \cdot 10^{-6}\right)^{0.6} \tag{90}$$

The second part of economic evaluation is the operating cost. This cost is estimated as follows:

a The amortization is calculated using eq. (77), considering 25 years of expected life for the A-frame bundles [19], and 18 years are considered for the fans and the cooling tower [43].
b The operating costs are estimated based on different factors for each system:
   - In the case of the A-frame this cost is due to the energy consumed by the fans, which can be calculated using eq. (78). The price of a kWh produced by a CSP plant is 0.083 $\$_{2013}$/kWh [46]. Part of that energy is consumed to operate the fans. The energy consumed considered has been computed in Section 4.2 for July.
   - In the case of the cooling tower, the operating cost is due to the losses of water by evaporation. The monthly consumption of water for the CSP plant considered in the analysis is $7.70 \cdot 10^{-3}$ m^3/s [47]. The price of water in Almería, the location selected for the CSP plant, is 1.204 607 €/m^3 [48].
2 The environmental evaluation focuses on computing the CO_2 emissions avoided by each of the systems. These emissions are calculated considering the equivalent amount of CO_2 generated if non-renewable resources had been used to produce the energy instead. However, from this value the generated by the fans consumption or by the water consumption must be subtracted. From the literature, it is assumed that each kWh obtained result in the emission of 0.632 kg CO_2 [49]:
   - In the case of the A-frame, the CO_2 emissions avoided corresponds to that produced by the CSP facility discounting the energy consumed power the fans, eq. (91):

Table 14
Economic and environmental evaluation.

Factor		Refrigeration system	
		A-frame	Humidification tower
Equipment cost	Core equipment ($\$_{2014}$)	175,078	1,854,379
	Fans ($\$_{2014}$)	2,053,355	–
Monthly equipment cost ($\$_{2014}$/month)		10,090	8,585
Water consumption ($\$_{2014}$/month)		–	33,035
Cost of energy consumption ($\$_{2014}$/month)		99 050	–
Total monthly cost ($\$_{2014}$/month)		**109,140**	**41,620**
CO_2 avoided emissions on July ($kgCO_2$)		**10981823.98**	**11724338.72**

$$Eco_{A-frame} = P_{gen} \cdot \left(744 \frac{kWh \cdot s}{kJ \cdot month}\right) \cdot \left(0.632 \frac{kgCO_2}{kWh}\right) \cdot \left(1 - \%_f\right) \tag{91}$$

- In the case of the cooling tower, the emissions mitigated are given by the power produced by the CSP facility minus those related to water consumption as presented in eq. (92). We assume that each m^3 of water used generates 0.30 kg CO_2 [50],

$$Eco_{tower} = P_{gen} \cdot \left(744 \frac{kWh \cdot s}{kJ \cdot month}\right) \cdot \left(0.632 \frac{kgCO_2}{kWh} - C_{H_2O} \cdot 0.30 \frac{kgCO_2}{m^3 H_2O}\right) \tag{92}$$

The results obtained for July are used to compute the CO_2 emissions and water and energy consumptions, see Table 14.

The A-frame option is, nowadays and for the location considered, worse solution than cooling towers under both criteria, cost and CO_2 emissions. The A-frame is worse because the use of fans raises the cost above that of the cooling towers and its low efficiency results in lower mitigation of CO_2 emissions. These results could change in the future if the following scenarios take place:

- The economic results of A-frame could be improved in three ways: by decreasing investment cost of the fans, and/or by increasing the fan mechanical efficiency and, with it, the mitigated emissions of CO_2. However, the price of water will increase in the future, due to the desertification [51], reducing the advantage of using cooling towers.
- The environmental results of A-frame could be improved if the cooling tower needs an additional fan system, because the CO_2 avoided emissions of this refrigeration system will decrease and the difference with the A-frame system will be lower.

Furthermore, in a previous paper [11] a correlation to define the selection of the cooling technology as a function of the water consumption and the energy produced was developed to evaluate the regions where one technology is preferable. The results presented above are in line with the predictions provided by that correlation supporting the use of wet cooling in the region of study.

6. Conclusions

In this work a two-stage optimization procedure for the design and monthly operation of A-frame dry cooling systems within solar thermal power plants has been developed. The particular features of these systems are the fact that the availability of water is limited as well as the variable production capacity over time as a function of solar incidence. A detailed model is developed as the basis for the optimization of the geometry including pipe number, layout, diameter and length. A MINLP problem is formulated and solved for the month of the largest cooling load, using a tailor-made branch and bound algorithm. In a second step, for the optimal geometry, we compute the optimal monthly use of the unit by formulating a multi-period MINLP. The solution of this problem indicates the use of number of fans, the air flowrate and its inlet and outlet temperature. The tool developed is detailed in the unit geometric characteristics and flexible to include new features or model for different fans.

The solution allows identifying several guidelines for the design of A-frames. It suggests an apex angle of 63°, one row of 75 pipes of 13.5 *m* long and with a diameter of 3.3 mm. A total of 4 fans are used but they only operate at full capacity during summer. This geometry shows a reduced consumption of energy by 0.7%, 20% less energy consumption that previous results, that within a power plant, results in a large energy savings. This two-step procedure reveals that multiperiod evaluation allows exploiting the design. It shows that it is recommendable to make full use of the temperature gradient to reduce the monthly air flow rate, saving energy on a monthly basis compared to a monthly optimization. Finally, the selection of cooling technology depends on the location because of water availability and weather conditions. Wet towers are quite competitive but CSP facilities are typically built in regions with limited water availability so that dry cooling systems are an interesting alternative.

Acknowledgement

The authors would like to acknowledge Salamanca Research for optimization software licenses. The authors acknowledge the TCUE fellowship from Fundación Universidad – Empresa USAL 2015 to Mr. JA Luceño.

Nomenclature

A_2	Entrance area of support structure, m^2
A_c	Total projected area of the fan, m^2
A_e	Effective area across the fan, m^2
A_f	Total outer fins' area, m^2
A_{fr}	Total frontal flow area, m^2
$A_{fr,bundle}$	Frontal flow area of a bundle, m^2
A_{in}	Inside total area, m^2
$A_{in,pipe}$	Inside area of a tube, m^2
A_k	Logarithm mean area, m^2
$A_{ob,do}$	Projected area of fan's downstream obstacles, m^2
$A_{ob,up}$	Projected area of fan's upstream obstacles, m^2
A_{out}	Outside total area, m^2
$A_{out,fin}$	Outer fin area, m^2
$A_{out,pipe}$	External total area of a pipe, m^2

A_{tf} Total fins area, m^2
A_{smooth} Smooth area of a tube, m^2
$Amort_{equipment}$ Amortization of an equipment, $\$_{2014}$/month
b_{fan} Bundles per fan
$C_{\$-kWh}$ kWh price, $\$_{2014}$/kWh
C_{Dts} Drag coefficient of support
C_{elec} Energy cost, $\$_{2014}$/month
$C_{equipment}$ Cost of an equipment, $\$_{2014}$
C_{fan} Cost of a fan, $\$_{2014}$
C_{frame} Heat exchanger cost, $\$_{2014}$
C_{H_2O} CO_2 generated by water, kg/m^3
$C_{p_{air}}$ Air heat capacity, kJ/(kg K)
$C_{p_{w,vap}}$ Water steam heat capacity, kJ/(kg K)
C_{tower} Cost of a humidification tower, $\$_{2014}$
d_c Inner fan diameter, m.
D_{eq} Equivalent diameter, m.
D_f Outer fin diameter, m.
d_{fh} Diameter of fan shaft, m
D_{in} Inner pipe diameter, m.
D_{out} Outer pipe diameter, m.
d_s Inlet steam duct diameter, m.
d_{ts} Width of support beam, m.
$DeLi_{equipment}$ Expected life of an equipment, year
e Pipe mean thickness, m.
$Eco_{A-frame}$ Avoided CO_2 emissions by an A-frame, $kgCO_2$
Eco_{tower} Avoided CO_2 emissions by a humidification tower, $kgCO_2$
f Binary parameter of the fan during the month
g Gravitational acceleration, m/s^2
H Humidity of the air, kg/kg
h_{air} Air side coefficient, kJ/(K m^2 s)
h_c Steam side coefficient, kJ/(K m^2 s)
$h_{ae}A_a$ hA steam term, kJ/(K s)
K_2 K_2 term of fan cost
k_{air} Thermal conductivity of air, kJ/(K m^2/m s)
k_c Thermal conductivity of saturated liquid water on steam temperature, kJ/(K m^2/m s)
K_{ci} Heat exchanger entrance contraction loss coefficient for normal flow
K_{dj} Coefficient of losses due to the turbulent decay of the jet after the bundles
K_{do} Pressure drop coefficient of fan's downstream obstacles
k_f Thermal conductivity of fin, kJ/(K m^2/m s)
K_{he} Loss coefficient for normal isothermal flow through the finned-tube bundle
k_{mat} Thermal conductivity of pipe material, kJ/(K m^2/m s)
K_o Coefficient of losses during the final mixing process as the flow leaves the A-frame
K_{ts} Pressure drop coefficient trough the support platform
K_{up} Pressure drop coefficient of fan's upstream obstacles
$K_{\theta t}$ Total pressure drop coefficient across the heat exchanger bundles
L_b Projected total length of pipe, m.
L_r Total bundle length, m.
L_s Projected free length of pipe, m.
L_t Pipe length, m.
L_{ts} Length of support beam, m.
L_w Walkway length, m.
$LMTD$ Logarithm mean temperature difference, K.
m Dimensionless term m
m_{air} Air mass flow, kg/s
m_{at} Equivalent air mass flow per tube of a pair of rows, kg/s
m_{fan} Air mass flow per fan, kg/s
m_w Water vapor mass flow, kg/s
N_b Number of bundles
n_b Number of bundles working corresponding to the studied fan
n_f Number of fins per tube
n_{fan} Number of fans
N_r Number of rows per bundle
N_t Number of pipes per row
n_{ts} Number of support beams per side.
Nu Nusselt number
Ny Characteristic heat transfer parameter of air, 1/m
p_f Separation between the same side of two adjacent fins, m.
P_F Power supplied by a fan on his shaft, kJ/s
P_{gen} Energy produced by the CSP, kJ/s
P_{vent} Total power supplied by fans, kJ/s
Pr Prandtl number
Q heat flow, kJ/s
Q_{air} Total air volume flow, m^3/s
Re Reynolds number
Ry Characteristic flow parameter of air, 1/m
Sep_{fan} Distance between fans, m.
$S_{\min-t}$ Minimum flow area, m^2
t_f Mean fin thickness, m.
$T_{in,air}$ Inlet air temperature, K.
$T_{out,air}$ Outlet air temperature, K.
T_v Water steam temperature, K.
U Overall heat transfer coefficient, kJ/(K m^2 s)
$U_cH_tL_t$ UHL steam term, kJ/(K s)
V_{air} Air volume flow per fan, m^3/s
v_{std} Air volume flow at standard conditions, m^3/s
x_{do} Downstream obstacles from the fan, m
X_l Horizontal tube pitch, m.
x_{up} Upstream obstacles from the fan, m
X_t Vertical tube pitch, m.
Z Objective function, $\$_{2014}$/month
$\%_f$ Percentage of energy consumed by fans

Greek letters

α_n Generic alpha-n parameter
β_n Generic beta-n parameter
Γ Airflow across the minimum flow area, kg/s
γ_{pt} Fan blade's angle, °.
Δp_e Total pressure drop across the system unit, Pa
Δp_{Fs} Fan static pressure, Pa
ΔT_a Temperature difference at the entrance of the heat exchanger, K.
ΔT_b Temperature difference at the exit of the heat exchanger, K.
ε_n Generic epsilon-n parameter
η_0 Outside area efficiency
η_f Fins' efficiency
η_{fan} Fan efficiency
θ A-frame apex angle, °.
θ_m Mean flow incident angle, °.
λ_w Latent heat of evaporation of the water steam, kJ/kg
μ_{air} Air viscosity, kg/(m s)
μ_c Saturated liquid water viscosity on steam temperature, kg/(m s)
ρ_{a3} Mean air density trough the fan, kg/m^3
ρ_{a56} Mean air density across the heat exchanger bundles, kg/m^3

ρ_c	Saturated liquid water density on steam temperature, kg/m^3
σ	Ratio of the minimum to free stream flow area through the heat exchanger bundle
σ_{21}	Ratio of the minimum to free stream flow area at the bundle inlet.
σ_c	Ratio of area related with K_{ci}
ϕ	Dimensionless term phi

Subscript

(m)	month

Superscript

i	i-th element of the set.
tot	Total monthly value of a variable

Appendix A. Supplementary data

Supplementary data to this article can be found online at https://doi.org/10.1016/j.energy.2018.09.177.

References

[1] González-Finat A, Liberali R. Concentrating solar power from research to implementation. Luxembourg, Luxembourg: Office for Official Publications of the European Communities; 2007.
[2] Martín L, Martín M. Optimal year-round operation of a concentrated solar energy plant in the south of Europe. Appl Therm Eng 2013;59:627–33.
[3] Kelly B, Price H. Nexant parabolic trough solar power plant systems analysis task 2: comparison of wet and dry rankine cycle heat rejection. San Francisco: Nexant Inc.: California; 2006.
[4] Turchi CS, Wagner MJ, Kutscher CF. Water use in parabolic trough power plants: summary results from WorleyParsons' analyses. Colorado, Golden: National Renewable Energy Laboratory; 2010.
[5] Zhai H, Rubin ES. Performance and cost of wet and dry cooling systems for pulverized coal power plants with and without carbon capture and storage. Energy Pol 2010;38:5653–60.
[6] Barigozzi G, Perdichizzi A, Ravelli S. Wet and dry cooling systems optimization applied to a modern waste-to-energy cogeneration heat and power plant. Appl Energy 2011;88:1366–76.
[7] Blanco-Marigorta AM, Sánchez-Henríquez MV, Peña-Quintana JA. Exergetic comparison of two different cooling technologies for the power cycle of a thermal power plant. Energy 2011;36:1966–72.
[8] Habl P, Blanco-Marigorta AM, Erlach B. Exergoeconomic comparison of wet and dry cooling technologies for the Rankine cycle of a solar thermal power plant. In: Proceedings of ecos; 2012. the 25th.
[9] Liqreina AALM. Evaluation of dry cooling option for parabolic trough [CSP] plants including related technical and economic assessment: case of study CSP Plant in Ma'an/Jordan. M.Sc. Thesis. Cairo University; 2012.
[10] Palenzuela P, Zaragoza G, Alarcón-Padilla DC, Blanco J. Evaluation of cooling technologies of concentrated solar power plants and their combination with desalination in the Mediterranean area. Appl Therm Eng 2013;50:1514–21.
[11] Martín M. Optimal annual operation of the dry cooling system of a concentrated solar energy in the south of Spain. Energy 2015;84:774–82.
[12] Esen Hikmet, Inalli Mustafa, Esen Mehmet. Technoeconomic appraisal of a ground source heat pump system for a heating season in eastern Turkey. Energy Convers Manag 2006;47:1281–97.
[13] Esen Hikmet, Inalli Mustafa, Esen Mehmet. A techno-economic comparison of ground-coupled and air-coupled heat pump system for space cooling. Build Environ 2007;42:1955–65.
[14] Esen Mehmet, Yuksel Tahsin. Experimental evaluation of using various renewable energy sources for heating a greenhouse. Energy Build 2013;65:340–51.
[15] Rosegrant MW, Cai X, Cline SA. Global water outlook to 2025: averting an impending crisis. Washington, DC: International Food Policy Research Institute; 2002.
[16] Dyreson A, Miller F. Night sky cooling for concentrating solar power plants. Appl Energy 2016;180:276–86.
[17] Chen L, Yang L, Du Xm, Yang Y. A novel layout of air cooled condenser to improve thermo flow performances. Appl Energy 2016;165:244–59.
[18] Yang LJ, Wang MH, Du XZ. Yang YP Trapezoidal array of air-cooled condensers to restrain the adverse impacts of ambient winds in a power plant. Appl Energy 2012;99:402–13.
[19] Zammit K. Air-cooled condenser design, specification, and operation guidelines. Palo Alto: Electric Power Research Institute: California; 2005.
[20] Heyns JA. Performance characteristics of an air-cooled steam condenser incorporating a hybrid (dry/wet) dephlegmator. M.Sc.E. Thesis. Stellenbosch, South Africa: University of Stellenbosch; 2008.
[21] Wolverine. Wolverine Tube Inc. Chapter 6 Heat transfer to air cooled heat exchangers. Engineering data book III. 2010. https://www.microcooling.com/wp-content/uploads/2012/09/DataBookIII.pdf http://www.wlv.com/heat-transfer-databook/Last. [Accessed June 2017].
[22] Butler C, Grimes R. The effect of wind on the optimal design and performance of a modular air-cooled condenser for a concentrated solar power plant. Energy 2014;68:886–95.
[23] Yang L, Zhao X, Du X, Yang Y. Heat load capability matching principle and its applications to anti-freezing of air cooled condenser. Appl Energy 2016;127:34–43.
[24] Bredell JR, Kröger DG. Numerical investigation of fan performance in a forced draft air-cooled steam condenser. California: California Energy Commission; 2006.
[25] Pieve M, Salvadori G. Performance of an air-cooled steam condenser for a waste-to-energy plant over its whole operating range. Energy Convers Manag 2011;52:1908–13.
[26] Manassaldi JI, Scenna NJ, Mussati SF. Optimization mathematical model for the detailed design of air cooled heat exchangers. Energy 2014;64:734–46.
[27] Conradie AE, Buys JD. Kroger DG Performance optimization of dry-cooling systems for power plants through sqp methods. Appl Therm Eng 1998;18(1–2):25–45.
[28] Grossmann IE, Halemane KP, Swaney RE. Optimization strategies for flexible chemical processes. Comput Chem Eng 1983;7(4):439–62.
[29] Kuruneru STW, Sauret E, Saha SC, Gu Y. Numerical investigation of the temporal evolution of particulate fouling in metal foams for air cooled heat exchangers. Appl Energy 2016;184:531–47.
[30] Chen JJ. Letter to the editor: comments on improvement on a replacement for the logarithmic mean. Chem Eng Sci 1987;42:2488–9.
[31] Towler G, Sinnott R. Chemical engineering design. Elsevier Inc.: United States of America; 2008.
[32] Kern DQ. Process de transferencia de calor (Process Heat Tansfer). Compañía Editorial Continental S.A.: México D.F.; 1999.
[33] Owen MTF. A numerical investigation of air-cooled steam condenser performance under windy conditions. M.Sc.E. Thesis. Stellenbosch, South Africa: University of Stellenbosch; 2010.
[34] Kröger DG. Air-cooled heat exchangers and cooling towers: thermal-flow performance evaluation and design, vol. II. Tulsa: Pennwell: Oklahoma; 2004.
[35] Daugherty RL, Franzini JB. Fluid mechanics with engineering applications. seventh ed. United States of America: McGraw-Hill Inc.; 1977.
[36] https://www.gerdau.com.co/Portals/4/CatalogoVigas.pdf [accessed February 2016).
[37] Llanos A. Personal communication. 2015.
[38] Perry RH, Green DW. Chemical engineers handbook. eighth ed. McGraw-Hill Education: United States of America; 2007.
[39] www.aemet.es/es/serviciosclimaticos/datosclimatologicos/valoresclimatologicos?l=6325O&k=and (accessed January 2013).
[40] Sancho Ávila JM, Riesco Martín J, Jiménez Alonso C, Sánchez de Cos Escuin MC, Montero Cadalso J, López Bartolomé M. Atlas de radiación solar AEMET (Spain) (AEMET solar radiation atlas: Spain). Madrid, Madrid: Agencia Estatal de Meteorología; 2013.
[41] www.agenciaandaluzadelaenergia.es/Radiacion/radiacion1.php (accessed January 2013).
[42] http://www.matche.com/equipcost/Exchanger.html (accessed February 2016).
[43] MPR, Ministerio de la Presidencia. Ley 24/2014, de 24 de noviembre, del Impuesto sobre Sociedades. Boletín Oficial del Estado 2014;288:96939–7097. . [Accessed February 2016].
[44] Walas SM. Chemical process equipment: selection and design. Boston: Butterworth-Heinemann; 1988.
[45] http://www.matche.com/equipcost/Cooling.html (accessed February 2016).
[46] https://www.eia.gov/forecasts/aeo/electricity_generation.cfm (accessed March 2016).
[47] Martín L. Planta de producción de energía por Concentración de energía Solar. Meng. Thesis. Salamanca, Spain: University of Salamanca; 2013.
[48] http://www.galasa.es/administracion/include/ficheros/documentos/20/Tarifas%20Galasa.pdf (accessed March 2016).
[49] Thomas C, Tennant T, Rolls J. The GHG indicator: UNEP guidelines for calculating greenhouse gas emissions for businesses and non-commercial organisations. United Nations Environment Programme; 2000.
[50] http://www.water.org.uk/news-water-uk/latest-news/water-industry-sustainability-latest-indicators (accessed March 2016).
[51] http://www.eea.europa.eu//publications/europes-environment-aoa (accessed January 2016).